© 2016. Published by The Company of Biologists Ltd | Journal of Cell Science (2016) 0, 1-16 doi:10.1242/jcs.188102

RESEARCH ARTICLE

Comparison of cancer cells in 2D vs 3D culture reveals differences in AKT–mTOR–S6K signaling and drug responses

Angelika Riedl[1,*], Michaela Schlederer[2,3], Karoline Pudelko[1], Mira Stadler[1], Stefanie Walter[1], Daniela Unterleuthner[1], Christine Unger[1], Nina Kramer[1], Markus Hengstschläger[1], Lukas Kenner[2,3,4], Dagmar Pfeiffer[5], Georg Krupitza[2] and Helmut Dolznig[1,‡]

ABSTRACT

Three-dimensional (3D) cancer models are used as preclinical systems to mimic physiologic drug responses. We provide evidence for strong changes of proliferation and metabolic capacity in three dimensions by systematically analyzing spheroids of colon cancer cell lines. Spheroids showed relative lower activities in the AKT, mammalian target of rapamycin (mTOR) and S6K (also known as RPS6KB1) signaling pathway compared to cells cultured in two dimensions. We identified spatial alterations in signaling, as the level of phosphorylated RPS6 decreased from the spheroid surface towards the center, which closely coordinated with the tumor areas around vessels *in vivo*. These 3D models displayed augmented anti-tumor responses to AKT–mTOR–S6K or mitogen-activated protein kinase (MAPK) pathway inhibition compared to those in 2D models. Inhibition of AKT–mTOR–S6K resulted in elevated ERK phosphorylation in 2D culture, whereas under these conditions, ERK signaling was reduced in spheroids. Inhibition of MEK1 (also known as MAP2K1) led to decreased AKT–mTOR–S6K signaling in 3D but not in 2D culture. These data indicate a distinct rewiring of signaling in 3D culture and during treatment. Detached tumor-cell clusters in vessels, in addition to circulating single tumor cells, play a putative role in metastasis in human cancers. Hence, the understanding of signaling in spheroids and the responses in the 3D models upon drug treatment might be beneficial for anti-cancer therapies.

KEY WORDS: AKT–mTOR–S6K signaling, MAPK signaling, Spheroid, Drug response

INTRODUCTION

Established cell lines have been essential in understanding the basic molecular principles of cancer (Bodnar et al., 1998; Hahn et al., 1999; Iyer et al., 1999). However, cancer cells have been continuously cultivated *in vitro* for a long time and have adapted to *in vitro* culture conditions. These concerns are often raised to question the relevance of cell lines as proper preclinical cancer models. However, for colorectal cancer (CRC), the analysis of the mutation and gene expression status of about 150 available human CRC cell lines has revealed that the entire variety of molecular and transcriptional subtypes, as previously described in CRCs *in vivo* (Marisa et al., 2013), is represented in this cell collection (Medico et al., 2015). In addition, these cells display the full range of drug responses to EGFR inhibition from sensitivity to resistance. Thus, CRC cell lines seem to fully cover the genetic, transcriptional and phenotypic make-up of cancer cells *in vivo*.

However, cells are often cultured as monolayers on flat surfaces, and these conditions do not faithfully reflect the situation *in vivo* given that proper tissue architecture and cell–cell contacts are lost in such two-dimensional (2D) systems. 3D cell cultures are well documented to regain intrinsic properties and to better mimic the *in vivo* situation than cells cultured as monolayers on plastic (Dolznig et al., 2011; Fischbach et al., 2009; Okawa et al., 2007; Pickl and Ries, 2009). Studies have shown that the gene expression profiles (Takagi et al., 2007) as well as the responses to treatment (Desoize and Jardillier, 2000) in the multicellular spheroid 3D models resemble more closely the *in vivo* situation. Similar to human tumors, proliferating, quiescent and dying cells coexist in normoxic, hypoxic or necrotic zones within spheroids (Hirschhaeuser et al., 2010). Therefore, 3D cancer models are increasingly recognized and biologically relevant for drug development and preclinical drug testing. *In vivo*, carcinoma cells not only form 3D structures but also interact with the surrounding extracellular matrix (ECM) and cells of the tumor stroma. These interactions have been shown to be essential for tumor development and progression, which prominently alter signaling pathways in both the tumor cells and the stromal cells.

Thus far, only a few comprehensive and systematic studies have been found that compare distinct signaling pathways in 2D vs 3D culture, in the presence or absence of ECM and/or stromal cells, or upon treatment with inhibitors (Ekert et al., 2014; Luca et al., 2013; Pickl and Ries, 2009). Changes in signaling cascades in cancer cells or crosstalk with other cell types in 3D cultures are still poorly understood. How these pathways change in response to targeted therapy and whether there is a different response in 2D vs 3D culture remain rather undocumented so far.

In this study, we systematically analyze the signaling changes in 2D vs 3D culture without adding further levels of complexity, such as the interaction of these cells with the ECM or stromal cells. We focus on the AKT and mammalian target of rapamycin (mTOR), and mitogen-activated protein kinase (MAPK) pathways because these two pathways are the most commonly mutated signaling routes in CRC and many other cancers. The PI3K–AKT–mTOR pathway is a central regulator of cell growth, proliferation, survival, metabolism and aging because it integrates different environmental cues. Dysregulation of the PI3K–AKT–mTOR pathway has been implicated in various pathological conditions, including cancer.

[1]Institute of Medical Genetics, Medical University of Vienna, Währinger Straße 10, Vienna A-1090, Austria. [2]Clinical Institute of Pathology, Medical University of Vienna, Währinger Gürtel 18-20, Vienna A-1090, Austria. [3]Ludwig Boltzmann Institute for Cancer Research, Währinger Strasse 13A, Vienna 1090, Austria. [4]Unit of Pathology of Laboratory Animals (UPLA), University of Veterinary Medicine Vienna, Vienna 1210, Austria. [5]Institute of Cell Biology, Histology and Embryology, Medical University of Graz, Harrachgasse 21, Graz 8010, Austria.
*Present address: Boehringer Ingelheim RCV GmbH & Co KG, Dr. Boehringer Gasse 5-11, Vienna A-1121, Austria.

‡Author for correspondence (helmut.dolznig@meduniwien.ac.at)

H.D., 0000-0002-6063-3585

Received 17 February 2016; Accepted 19 September 2016

Journal of Cell Science (2016) 0, 1-16 doi:10.1242/jcs.188102

Based on these findings, different efforts to modulate the PI3K–AKT–mTOR activity by pharmacologically targeting different molecules in the pathway are ongoing (Laplante and Sabatini, 2012).

We provide here some evidence of significant differences in PI3K–AKT–mTOR signaling in a 3D vs a 2D system, including spatial alterations in the signaling strength and responses upon treatment with inhibitors of the AKT, mTOR and S6K (also known as RPS6KB1) axis or of the MAPK (ERK) axis.

RESULTS

Colon cancer cells grown as spheroids display significantly reduced cell cycle progression

We used six colon cancer cell lines in this study. Caco-2 cells display enterocyte-like differentiation and do not harbor known mutations in the PI3K–AKT–mTOR or RAS–RAF–MAPK pathways (Hidalgo et al., 1989; Pinto et al., 1983). LS174T, DLD-1 and HCT116 cells contain mutations in both PI3K and KRAS, HT29 cells have mutations in BRAF and PI3K, and SW620 cells are driven by mutant KRAS (Table S1).

All cell lines formed spheroids within 24–48 h after seeding. Spheroid morphology varied from a compact appearance (DLD-1, HT29) and less-condensed spheroids with smooth (HCT116) or irregular surfaces (LS174T) to loose aggregates (SW620) and adenomatous cell clusters (Caco-2) (Fig. 1A). EdU-incorporation was used to precisely determine the cell cycle distribution of cells grown in 2D or 3D culture (Fig. 1B). A significant reduction (−50%) of cells in S-phase in 3D culture compared to those in 2D culture was observed in HT29, HCT116, Caco-2 and DLD-1 cells. A small reduction (−20%, Fig. 1C) in the number of cells in S-phase was observed in LS174T and SW620 cells. Cell death, as determined by calculating the percentage of subG1 cells by flow cytometry, was generally low in all cell lines when cultured in three or two dimensions (Fig. 1D). Nevertheless, there was a twofold increase in the apoptotic rate in 3D culture compared to the rate in 2D culture of DLD-1 cells (8% and 4% in 3D and 2D culture, respectively). Low levels of apoptosis were confirmed by cleaved-caspase-3 staining in 2D culture as well as in spheroid sections (Fig. 1E). No spatial variations were detected in the spheroids – apoptotic cells appeared randomly without clustering in specific areas.

Spheroid culture of CRC cells is associated with diminished AKT–mTOR–S6K signaling

Next, we determined the molecular differences in signaling pathways in the CRC cells in 2D and 3D culture by using western blot analysis (Fig. 2A). The amount of phosphorylated (phospho) proteins was quantified by using densitometry evaluation (Fig. 2B) of three biological replicates. Phosphorylation of pan-AKT at residue S473 (referring to the position of serine in AKT1; phospho-AKT) was weak in SW620 cells compared to that in the other cell lines. Diminished phospho-AKT corresponded to low AKT activity, as observed by the reduced phosphorylation of the direct AKT target PRAS40 (also known as AKT1S1). Interestingly, in five cell lines (LS174T, HT29, HCT116, Caco-2, DLD-1), AKT phosphorylation was selectively reduced in 3D but not in 2D culture. This was associated with decreased phospho-PRAS40 in four of the five cell lines (i.e. cell lines LS174T, HT29, HCT116, DLD-1); in Caco-2 cells, PRAS40 was equally phosphorylated during 2D and 3D culture (Fig. 2B upper panels). In all six lines tested, S6K and RPS6 phosphorylation was consistently and significantly reduced in spheroids, which indicated reduced mammalian target of rapamycin complex 1 (mTORC1) activity. Accordingly, another direct target of mTORC1, eukaryotic initiation factor 4 binding protein 1 (4E-BP1), was less phosphorylated under 3D culture. The level of hyperphosphorylated 4E-BP1 (i.e. 4E-BP1γ) was reduced to about 50% in LS174T, HT29, Caco-2 and DLD-1 cells cultured in 3D as compared to that under 2D culture, or by 20% in SW620; no change in HCT116 cells was found (Fig. 2B, middle panels). In contrast, phosphorylation of MAPK3 and MAPK1 (phospho-ERK1/2) as an indicator of active RAS–RAF–MAPK signaling was variably influenced by 3D culture conditions. In DLD-1, LS174T and HT29 cells, ERK1/2 phosphorylation remained unchanged in 3D compared to 2D culture. Phospho-ERK1/2 was significantly induced in SW620 and Caco-2 cells in 3D culture but decreased in HCT116 cells. PKCβII (an isoform encoded by *PRKCB*) phosphorylation was slightly (LS174T, HCT116, DLD-1, HT29) or strongly induced (SW620, Caco-2) in 3D culture, indicating that there was not a general decrease in phosphorylated proteins, thereby ruling out a handling, harvesting or cell lysis artifact that was only present in 3D cultures (Fig. 2B, lower panel).

In summary, these experiments reveal a general profound and highly specific decrease in AKT–mTOR–S6K signaling in cancer cells grown as spheroids as compared to those cultured in the respective conventional 2D system.

Phenotypic analysis of CRC cells in 2D and 3D culture upon treatment with specific kinase inhibitors

The global decrease in the activity of the AKT–mTOR–S6K axis in 3D cultures prompted further investigation of specific inhibitors that target major hubs in this pathway and comparison of the phenotypic changes, as well as molecular responses in signaling, in 2D vs 3D cultures. A MAPK pathway inhibitor targeting MEK1 (also known as MAP2K1) was also included. The inhibitors used in this study were rapamycin, Torin1, PF4708671, MK2206 and AZD6244 to target mTORC1, mTOR, S6K, AKT and MEK1 kinase activities, respectively. DLD-1, Caco-2 and HCT116 were selected for this in depth analysis because these cell lines belong to the same transcriptional subtype of CRC cells (stem-cell like; Marisa et al., 2013; Medico et al., 2015). DLD-1 and HCT116 harbor the same mutations in the PI3K–AKT and MAPK pathways, whereas Caco-2 cells are wild type for those pathways.

Cells were grown in 2D or 3D culture for 1 day and were treated with compounds or solvent control (DMSO) for another 24 h. Proper drug action was verified by western blot analysis of key phospho-proteins in the disrupted signaling pathway. Upon treatment with rapamycin, PF4708671, MK2206 or AZD6244, cell morphology of DLD-1 cells (Fig. 3A) in 2D culture was unchanged. In contrast, DLD-1 spheroids that had been treated with Torin1, MK2206 and AZD6244 appeared darker in phase contrast analyses (Fig. 3A). In comparison to DMSO controls, spheroid size was reduced to about 50% upon treatment with Torin1, and the rapamycin-, MK2206- or AZD6244-treated spheroids displayed intermediate volume reduction (75% of controls), whereas PF4708671 had a small but significant impact on spheroid size (Fig. 3A,B). The volume of HCT116 spheroids was reduced significantly under all treatment conditions. In Caco-2 spheroids, treatment with Torin1 and MK2206 resulted in spheroids that were 80% of the size of controls (Fig. S1A,B).

Cell cycle analysis revealed essential differences in treatment responses between DLD-1 cells that had been cultured in two vs three dimensions (Fig. 3C; HCT116 and Caco-2, Fig. S1C). In the 2D system, rapamycin, PF4708671 and AZD6244 had no effect on cell cycle progression, whereas Torin1 reduced the proportion of cells in S-phase to less than 15% as compared to 38% in DMSO

Journal of Cell Science (2016) 0, 1-16 doi:10.1242/jcs.188102

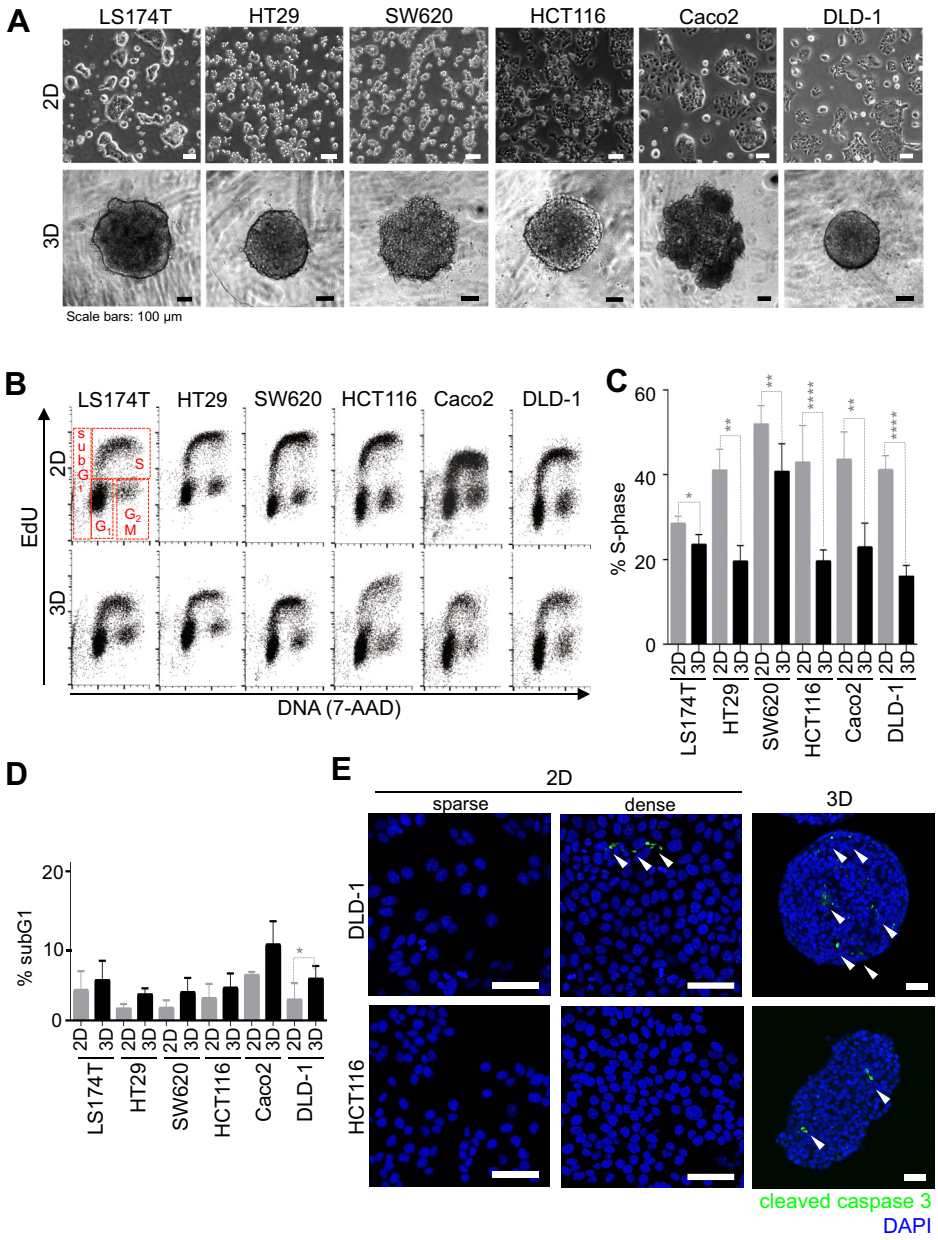

Fig. 1. Analysis of morphology and cell cycle in 2D vs 3D cell cultures. LS174T, HT29, SW620, HCT116, Caco-2 and DLD-1 colon cancer cells were grown as monolayers or spheroids (3000 cells/spheroid). After 48 h, cells and spheroids were photographed and cell cycle analysis was performed. (A) Representative microscopy images of colon cancer cells in 2D and 3D cultures. (B) Cell cycle analysis of monolayer cells and spheroids using EdU and 7AAD. The percentages of cells in S-phase (C) and sub-G1 (D) (boxed in red for LS174T cells in B) were determined (LS174T, n=4; HT29, n=3; SW620, n=6; HCT116, n=8; Caco-2, n=4; DLD-1, n=9 replicates per condition). Bars are mean±s.d.; Student's t-test (unpaired, two-tailed); *$P\leq0.05$, **$P\leq0.01$, ****$P\leq0.0001$. Detailed cell cycle analysis is available in supporting figure 2. (E) Cleaved-caspase-3 (green) staining in 2D cultures and spheroid sections. White arrowheads indicate apoptotic cells; DAPI, blue. Sparse, 30% confluent; dense, 90% confluent. Scale bars: 100 µm.

controls. Inhibition of AKT had a small but significant effect on proliferation. In contrast, cell proliferation was affected by all compounds (except for the S6K inhibitor) in the 3D model. MK2206 displayed a more pronounced inhibitory effect by reducing the number the cells in S-phase by 50% (8% vs 16%). Unexpectedly, AZD6244 was even more effective, resulting in only 4% of cells replicating; however, it was ineffective in 2D cultures. Interestingly, total inhibition of mTOR kinase activity led to a complete block in cell proliferation in 3D culture (0.3% of cells were in S-phase), whereas blocking mTORC1 activity with rapamycin had a minor effect (10% vs 16% in controls). HCT116 cells were most effectively slowed down in their proliferation through inhibition of S6K and MEK1 in 2D culture. However, in 3D cultures, AZD6244 and Torin1 treatment resulted in the most pronounced effects on proliferation (Fig. S1C), as also seen in DLD-1 and Caco-2 spheroids (Fig. S1C).

To further corroborate these findings, cellular metabolic capacity was determined (Fig. 3D), which faithfully recapitulated the pattern of the cell cycle analysis in DLD-1 and HCT116 cultures. Interestingly, there was a general decrease in metabolic activity of cells in 3D compared to 2D cultures – a 40% decrease was observed for DLD-1 cells in 3D culture (Fig. 3D) and a 60% decrease in HCT116 and Caco-2 cells (Fig. S1D). Subtle but significant differences were detectable, similar to results observed in the cell cycle analysis. All treatments that appeared to have no effect on proliferation in 2D and in 3D culture (see Fig. 3C; Fig. S1C) nevertheless resulted in small decreases in metabolic activity. Surprisingly, this was not the case in Caco-2 cells in which the level of intracellular ATP was rather inversely correlated with the S-phase data.

As inhibition of the mTOR pathway results in reduced cellular volume (Fingar et al., 2002), we next determined whether a gross decrease of cell size contributes to the effects of the inhibitors on spheroid size. Cell size was reduced by Torin1 in DLD-1 (Fig. 3G), HCT116 (Fig. S1F) and Caco-2 spheroids (Fig. S1F), or in the 2D system only marginally.

Journal of Cell Science (2016) 0, 1-16 doi:10.1242/jcs.188102

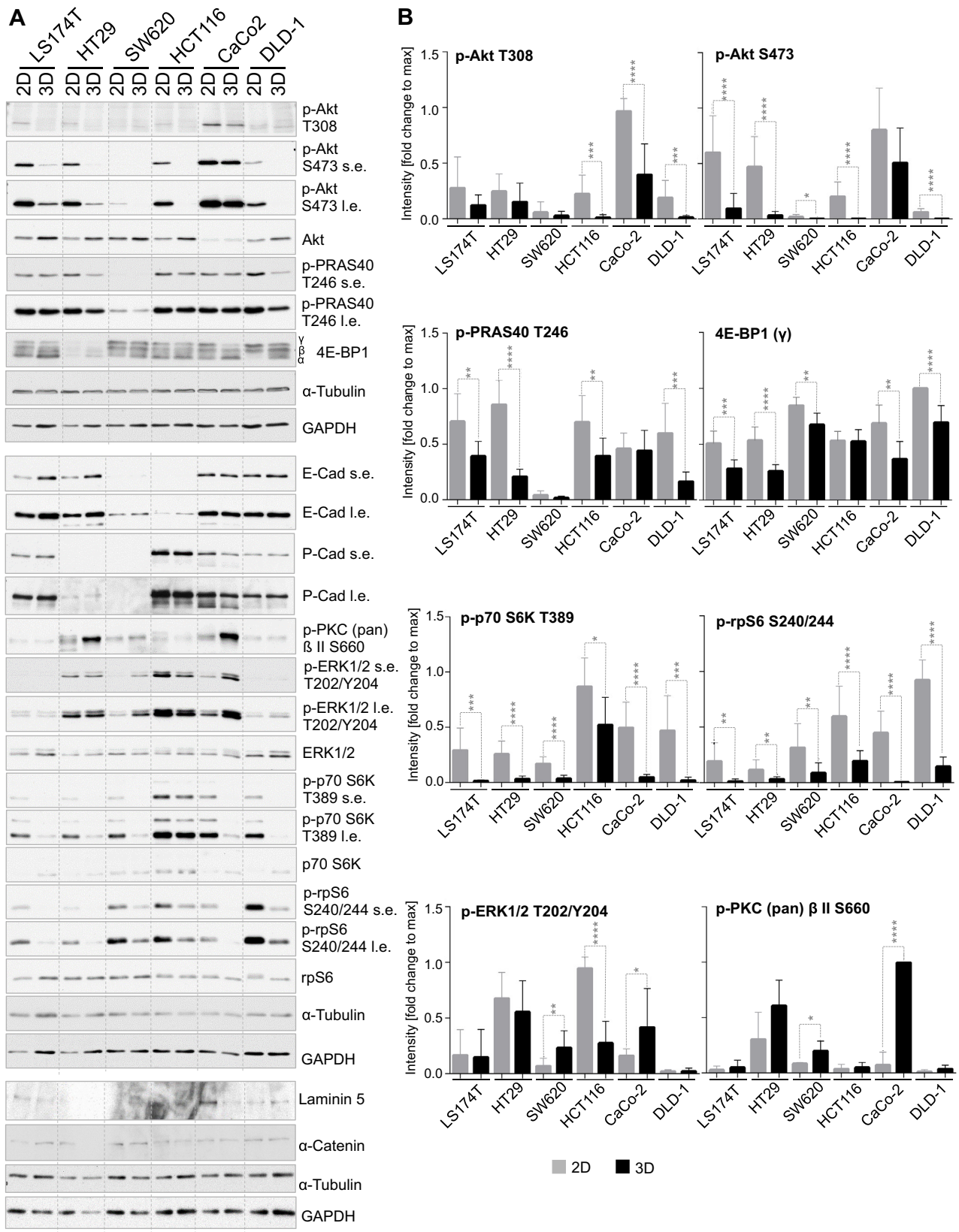

Fig. 2. PI3 K–AKT–mTOR and RAS–RAF–MAPK signaling in 3D spheroids compared to 2D cultures. The indicated cells were cultured in two and three dimensions for 48 h. Cells and spheroids (3000 cells/spheroid) were harvested and (A) immunoblot analysis of different proteins of the PI3K–AKT–mTOR and RAS–RAF–MAPK pathway was performed. Detection of phospho-proteins is indicated by the prefix 'p-' and the phosphorylated residue is stated. α-tubulin and GAPDH are loading controls. Cad, cadherin; l.e., long exposure; s.e., short exposure. (B) The protein levels in 2D and 3D cultures by western blotting (shown in A) were evaluated by using densitometry (n=6–12 replicates per condition, three independent experiments, additional blots are shown in supporting figure 1). Bars are mean integrated density±s.d. Student's t-test (unpaired, two-tailed); *$P\leq0.05$, **$P\leq0.01$, ***P≤0.001, ****$P\leq0.0001$.

Journal of Cell Science (2016) 0, 1-16 doi:10.1242/jcs.188102

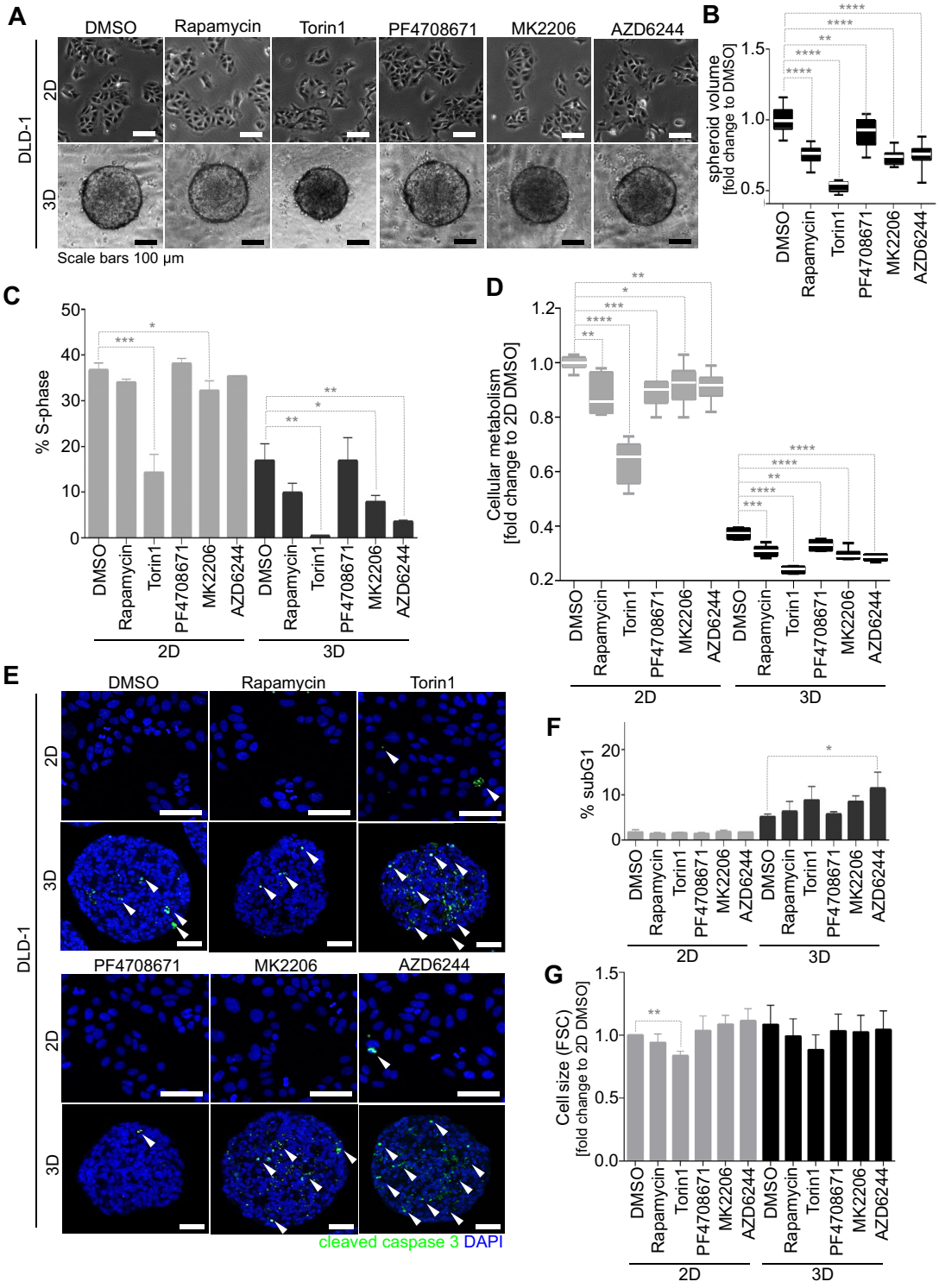

Fig. 3. Morphologic and phenotypic responses of colon cancer cells to inhibitor treatment in 2D vs 3D culture. DLD-1 cells were grown as a monolayer or spheroids (3000 cells/spheroid) for 24 h and further cultured in the presence or absence of rapamycin (100 nM), Torin1 (250 nM), PF4708671 (10 µM), MK2206 (1 µM) and AZD6244 (1 µM) for 24 h. DMSO served as control. (A) Representative microscopy images of control and treated DLD-1 cells in 2D and 3D cultures are shown. (B) The volume of spheroids was calculated and normalized to that of DMSO controls (four independent experiments, *n*=18 spheroids per condition). (C) Cell cycle analysis was performed using EdU and 7AAD, and the percentage of cells in S-phase is shown (*n*=3 replicates per condition). (D) Cellular metabolic capacity (intracellular ATP) was evaluated in DLD-1 (*n*=6 replicates per condition). (E) Cleaved-caspase-3 staining (green) in DLD-1 cells in 2D and 3D cultures. White arrowheads indicate apoptotic cells. Nuclear stain, DAPI, blue. Data for HCT116 cells are shown in supporting figure 3. Scale bars: 100 µm. (F) Quantification of dead cells by performing sub-G1 content analysis; *n*=3 replicates. (G) Cell size was determined by forward scatter (FSC) and normalized to that of the 2D-cultured DMSO controls (*n*=3 replicates per condition). Bars are mean±s.d. (B,D) The box ranges from the lower (quartile 1) to the upper quartile (quartile 3) in box and whisker plots; horizontal line, median; whiskers extend to the minimum and maximum. Student's *t*-test (unpaired, two-tailed); **P*≤0.05, ***P*≤0.01, ***P≤0.001, *****P*≤0.0001.

Journal of Cell Science (2016) 0, 1-16 doi:10.1242/jcs.188102

Apoptosis levels remained low under treatment with compounds, as determined by staining of cleaved caspase-3 (DLD-1, Fig. 3E) and sub-G1 DNA content (DLD-1, Fig. 3F; HCT116, Caco-2, Fig. S1E). Single inhibitor treatment had no gross apoptotic effect on the CRC cells either in 2D or in 3D culture, which is indicated by the low percentage of cells in sub-G1. Interestingly, only inhibition of MEK1 (by AZD6244) induced low rates of apoptosis in 3D culture compared to the controls. Thus, the small differences in cell size and apoptosis led to the conclusion that reduced spheroid volume, which might serve as an approximation for impaired tumor growth, is predominantly due to a reduction of cellular proliferation capacity under effective treatment conditions. Taken together, there are sharp differences in drug responses in 2D vs 3D culture. Inhibition of mTOR(C1)–AKT resulted in more severe anti-proliferative activity in 3D spheroids as compared to that in the 2D system.

Altered signaling in 2D vs 3D cultures upon AKT–mTOR and/or MAPK pathway inhibition

In addition, treated cells in 2D and 3D culture were analyzed for total and phosphorylated proteins involved in AKT–mTOR and MAPK signaling by western blotting. Three biological replicates were analyzed (DLD-1, Fig. 4A), and the mean response was calculated by performing densitometry evaluation (Fig. 4B; Fig. S2). Firstly, this was conducted to demonstrate proper drug action, and secondly, to identify differences in signaling upon inhibitor treatment between 2D and 3D cultures. In all three cell lines, treatment with rapamycin and Torin1 resulted in complete abrogation of phospho-S6K in 2D and 3D cultures, whereas Torin1 further inhibited AKT phosphorylation as a result of mTORC2 blockade. There was a consistent increase in phospho-AKT (residue S473) in the presence of rapamycin or PF4708671, which is indicative of the discontinuation of the negative feedback loop to IRS1 as a result of these two inhibitors (Tremblay et al., 2007). Treatment with PF4708671 led to an accumulation of phospho-S6K, which has been shown to lack kinase activity (Pearce et al., 2010), and further downstream, to a decreased level of phospho-RPS6. Treatment with MK2206 abolished AKT phosphorylation at S473 and T308, and the phosphorylation of the downstream target PRAS40 was eliminated.

Of note, upon MK2206 and AZD6244 treatment, the levels of phospho-S6K and phospho-RPS6 were decreased in spheroids, but not in the 2D cultures, indicating a response of mTORC1 activity to AKT or MEK1 inhibition only in the 3D model. Furthermore, abrogating the AKT–mTOR–S6K axis with any inhibitor increased ERK1/2 phosphorylation effectively in the 2D, but not in the 3D, model.

In conclusion, these data reveal that mTOR activity and the crosstalk between AKT–mTOR–S6K signaling and the MAPK pathway is altered in 3D compared to 2D cultures.

Spatial differences of signaling strength account for reduced S6K phosphorylation in spheroids and faithfully recapitulate the *in vivo* situation

The prominent decrease of phospho-RPS6 in spheroids in western blots could be due to two reasons. Either phospho-RPS6 is reduced in every cell to a similar extent or there are cells with variable expression levels from high to low or absent, which in sum give rise to the diminished phospho-RPS6 levels detected by immunoblotting.

Immunofluorescence analysis (Fig. 5A) confirmed the signaling response to treatment with inhibitors observed by western blotting analysis. In 2D culture, treatment with rapamycin, Torin1 and, to a lesser extent, PF4708671 led to a reduction of phospho-RPS6. Cross-sections of cells grown in two dimensions showed the same result (supporting figure 7). DLD-1 cells that had been treated with MK2206 or AZD6244 in 2D cultures showed no decrease in phospho-RPS6. However, the spheroid sections that had been stained for phospho-RPS6 revealed uneven intensities. A clear gradient of phospho-RPS6 staining intensity from the spheroid surface to the inner core was evident in the controls. This was also seen at reduced levels in PF4708671-, MK2206- and AZD6244-treated spheres. However, the staining inside displayed more variation than that in DMSO controls (Fig. 5A), whereas Torin1 and rapamycin diminished phospho-RPS6 almost completely. Total RPS6 protein was not affected and was expressed at high levels in every cell (Fig. S3A,B).

As a more objective evaluation, image analysis was used (Schlederer et al., 2014). Automated spheroid recognition and zonation (Fig. 5B, Fig. S3C) allowed division of equatorial sphere sections into three zones – an outer zone comprising the surface two-cell layers followed by a middle zone and the inner core (Fig. 5C). Nuclear recognition and creation of a cytoplasmic mask was used to quantitatively determine phospho-RPS6 levels in every single cell in the three distinct zones. In DMSO controls, the outer rim displayed a mean phospho-RPS6 level of 100 (Fig. 5D). In the inner core, phospho-RPS6 was reduced to more than half, and in the middle zone, a mean value of 63 was determined, which indicated a non-linear rapid decrease of S6K phosphorylation from the surface to the center (Fig. 5D). In rapamycin- or Torin1-treated spheroids, there was an almost complete loss of S6K phosphorylation in all zones. S6K, AKT and MEK1 inhibition resulted in a gradient similar to that in the control but with reduced mean intensities. Interestingly, the range of the signals varied from 200 to 25 under MK2206 and AZD6244 treatment in the outer zone, indicating that some cells still displayed maximal phospho-RPS6 levels in this area, comparable to DMSO controls, whereas the minimum was reduced to half. Inhibition of S6K reduced the range of phospho-RPS6 levels from 150 to 25, and the mean was smaller than that with the AKT or MEK1 inhibitors, suggesting that RPS6 phosphorylation was reduced in all cells (Fig. 5D).

Importantly, phospho-RPS6 gradients in *in vivo* DLD-1 xenografted tumors were present as detected in the DMSO-treated control spheroids (Fig. 5E), underscoring the ability of our model system to faithfully recapitulate the *in vivo* situation for AKT–mTOR–S6K signaling. *In vivo*, the highest levels of RPS6 phosphorylation were evident in the direct vicinity of cross-sectioned perpendicular tumor blood vessels. The levels of phospho-RPS6 radially diminished with increasing distance to the endothelium (Fig. 5E). Total RPS6 signals were invariably present in all cells (Fig. S4A). In the DLD-1 xenograft, cellular phospho-RPS6 signals were quantified in vessel-proximal, intermediate and vessel-distal zones (Fig. 5F). This analysis revealed an astonishingly similar pattern of intensity distributions, with highest levels of phospho-RPS6 in a vessel-proximal area that was three-cell-layers thick, and a prominent drop in the intermediate layer and low-to-absent vessel-distal signals (Fig. 5G). On the one hand, this qualifies DLD-1 spheroids as a reliable model for physiological mTOR–S6K signaling in tumors. On the other hand, it reveals that growth factor, nutrient and/or oxygen gradients are a probable explanation for the formation of the gradient from the surface to the center of the spheroid.

However, this recapitulation of the *in vivo* data by the *in vitro* assay might be specific for DLD-1 cells and thus be of limited

Journal of Cell Science • Advance article

Journal of Cell Science (2016) 0, 1-16 doi:10.1242/jcs.188102

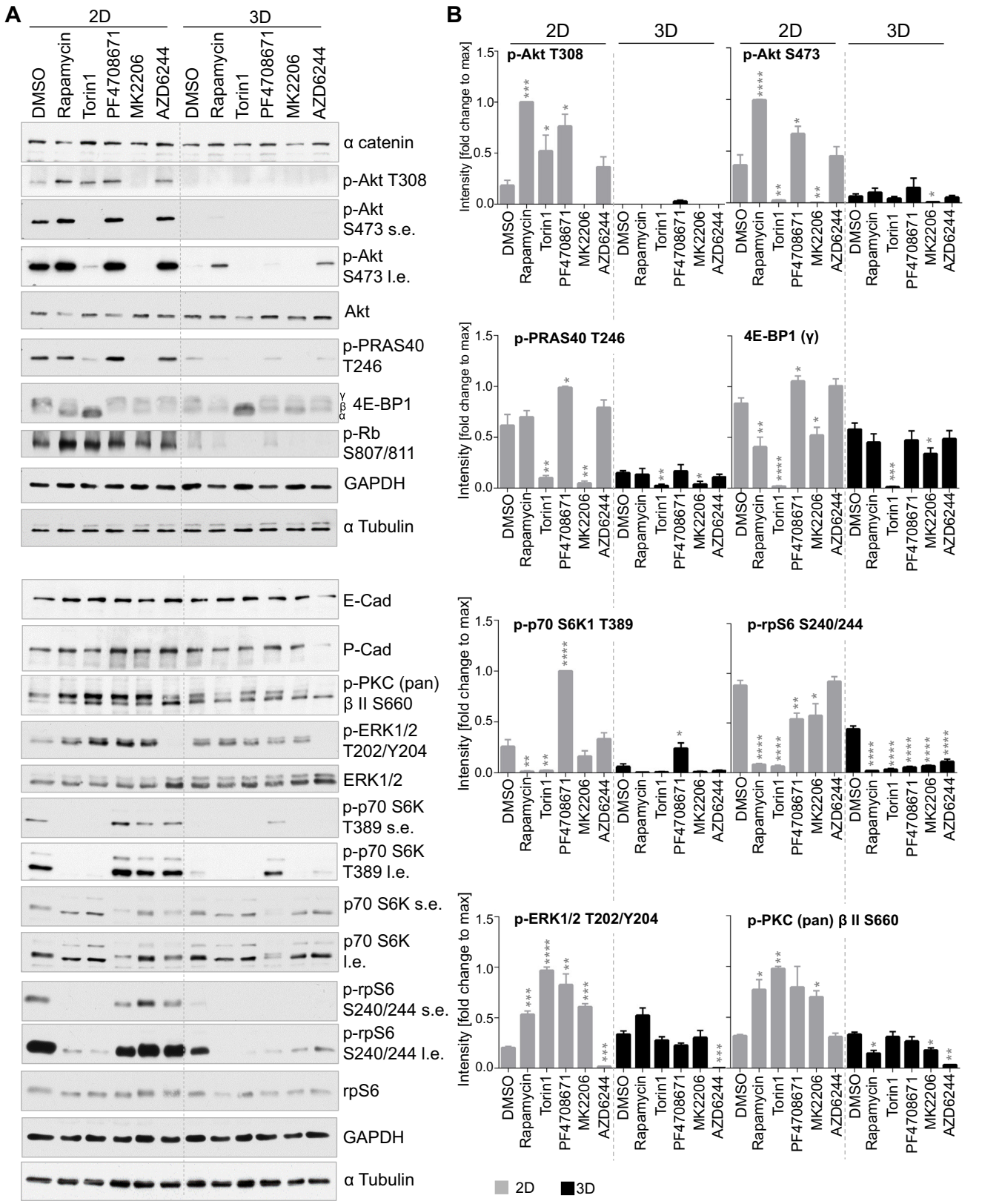

Fig. 4. PI3K–AKT–mTOR and RAS–RAF–MAPK signaling in the presence or absence of inhibitory compounds. DLD-1 colon cancer cells that had been pre-grown in 2D and 3D cultures (3000 cells/spheroid) for 24 h were treated with DMSO, 100 nM rapamycin, 250 nM Torin1, 10 µM PF4708671, 1 µM MK2206 and 1 µM AZD6244 for 24 h. 2D and 3D cultures were harvested and subjected to (A) immunoblot analysis. Detection of phospho-proteins is indicated by the prefixed 'p-' and the phosphorylated residue(s) are indicated. α-tubulin and GAPDH served as loading controls. l.e., long exposure; s.e., short exposure. HCT116 and Caco-2 data are shown in supporting figures 5 and 6. (B) The bands in western blots from three independent experiments (shown in A and supporting figure 4) were evaluated by using densitometry (n=2–8 replicates per condition). The data for HCT116 and Caco-2 are depicted in Fig. S2. Bars are mean integrated density±s.e.m. Student's t-test (unpaired, two-tailed); *P≤0.05, **P≤0.01, ***P≤0.001, ****P≤0.0001.

Journal of Cell Science (2016) 0, 1-16 doi:10.1242/jcs.188102

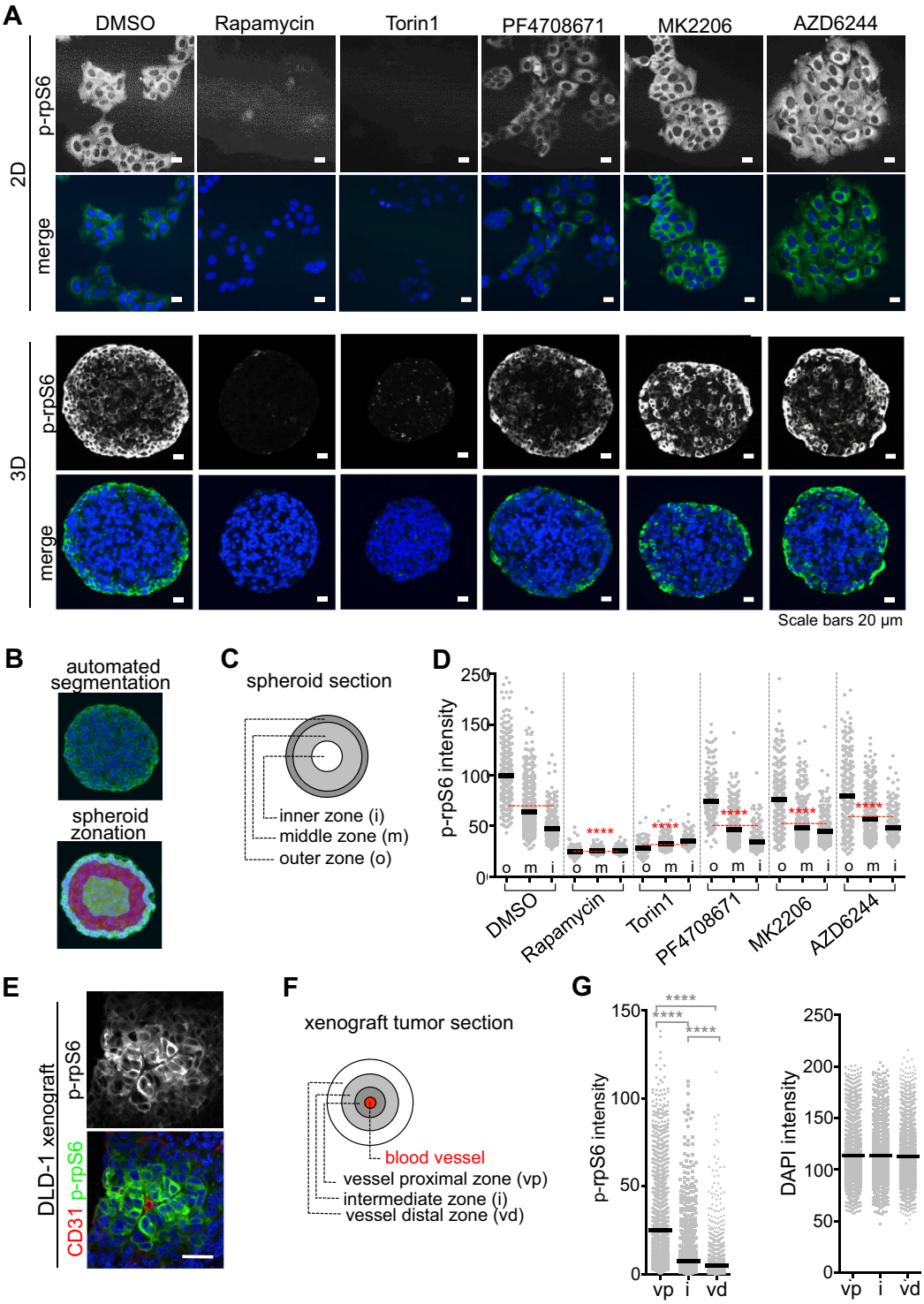

Fig. 5. Gradual decrease of RPS6 phosphorylation from the outside to the inner core of DLD-1 spheroids, and from vessel-proximal to vessel-distal areas of DLD-1 tumors grown *in vivo*. DLD-1 colon cancer cells were grown in 2D and 3D (3000 cells/spheroid) conditions for 24 h and treated with DMSO, 100 nM rapamycin, 250 nM Torin1, 10 µM PF4708671, 1 µM MK2206 and 1 µM AZD6244 for another 24 h. (A) Confocal images of DLD-1 cells in 2D or 3D cultures (5 µm sections) stained for phospho (p)-RPS6 at residues S240 and S244 (white, green in merge). Nuclei, blue, DAPI. Representative images are shown. See also Fig. S3A. (B) Image analysis by segmentation and spheroid recognition with the StrataQuest software allowed for automated spheroid zonation into three areas. (C) Spheroids were separated into an outer (o), middle (m) and inner (i) zone, and cell fluorescence signals were measured (minimum of five sections from different spheroids; cell numbers, n=157–803 per condition). (D) The mean phospho-RPS6 (residues S240 and S244) fluorescence intensity of all individual DLD-1 cells in spheroids was quantified using StrataQuest software. Scatter plots are shown; individual data points are shown (gray dots), and the horizontal black lines indicate means. A red-dotted line depicts the mean calculated from all three areas. Significant differences of these means compared to those of DMSO controls are indicated by red stars. Student's t-test (unpaired, two-tailed); ****$P\leq0.0001$. (E) Staining of phospho-RPS6 (residues S240 and S244; green), CD31 (red) and nuclei (DAPI, blue) in a DLD-1 xenograft tumor (5-µm sections). (F) For quantification, xenograft tumors were separated into vessel-proximal (vp), intermediate (i) and vessel-distal (vd) zones. (G) Quantification of mean phospho-RPS6 (at residues S240 and S244) and DAPI intensity in DLD-1 xenograft tumors (three animals; 15 tumor regions; cell numbers analyzed, n=3128–3372) using StrataQuest. Representative images are shown in Fig. S4A. Student's t-test (unpaired, two-tailed); ****$P\leq0.0001$.

Journal of Cell Science (2016) 0, 1-16 doi:10.1242/jcs.188102

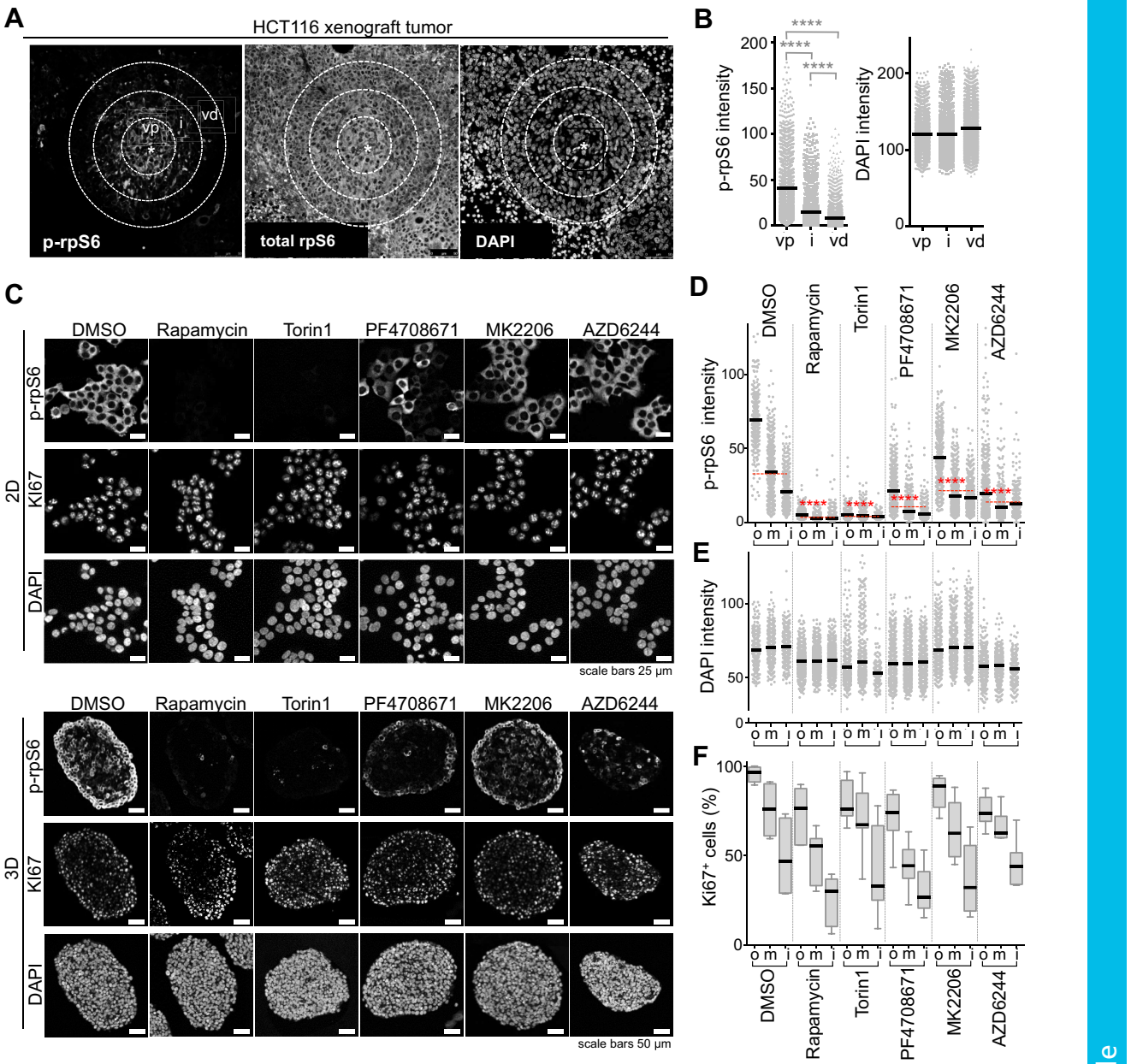

Fig. 6. Phospho-RPS6 levels and Ki67 positivity in HCT116 spheroids compared to 2D monolayers and HCT116 xenografts in mice. (A) Staining of phospho (p)-RPS6 (residues S240 and S244), total RPS6 and nuclei (DAPI) in a HCT116 xenograft tumor (5-µm sections). For quantification, xenograft tumors were separated into a vessel-proximal (vp), an intermediate (i) and a distal-vessel (dv) zone (white-dotted circles). The position of the vessel is indicated by *. (B) Quantification of mean phospho (p)-RPS6 (S240 and S244) and DAPI fluorescence intensities in HCT116 xenograft tumors (three animals; 23 tumor regions; individual cells analyzed, *n*=2714–3484) using the StrataQuest software in vessel-proximal (vp), intermediate (i) and vessel-distal (vd) zones. Representative images are shown in Fig. S4B. Horizontal black lines indicate means. (C) HCT116 cells were grown in 2D and 3D (3000 cells/spheroid) conditions for 24 h and treated with DMSO, 100 nM rapamycin, 250 nM Torin1, 10 µM PF4708671, 1 µM MK2206 and 1 µM AZD6244 for another 24 h. Immunofluorescence staining of p-RPS6 (S240 and S244) and Ki67 of HCT116 cells in 2D or 3D cultures (5-µm sections). Nuclei were counterstained with DAPI. Representative confocal images are shown. Scale bars: 25 µm (2D); 50 µm (3D). (D,E) The mean p-RPS6 (S240 and S244) and DAPI fluorescence intensities of all individual HCT116 cells in spheroids were quantified using the StrataQuest software. Spheroids were separated into an outer, middle and inner zone, and fluorescence signals were measured (minimum of five sections from different spheroids analyzed; cell number, *n*=170–1161 per condition). Scatter plots are shown; individual data points are shown (gray dots), and the horizontal lines indicate means. The mean calculated from all three areas is indicated by a red dotted line. Significant differences of these means compared to those of DMSO controls are indicated by red stars. Student's *t*-test (unpaired, two-tailed); *$P \leq 0.05$, **$P \leq 0.01$, ***$P \leq 0.001$, ****$P \leq 0.0001$. (F) Box and whisker plots represent the percentage of Ki67-positive (Ki67$^+$) cells in HCT116 spheroids, which were separated into an outer, middle and inner zone, as in D. The box ranges from the lower (Q1) to the upper quartile (Q3) in box and whisker plots; horizontal line, median; whiskers extend to the minimum and maximum.

relevance. Hence, the experiments were repeated with HCT116 cells, which differ in their mutational status from DLD-1 cells (Table S1). Indeed, the phospho-RPS6 gradient around blood vessels was confirmed in HCT116 xenografts (Fig. 6A,B), and the gradual decrease of phospho-RPS6 from outside to inside was corroborated in HCT116 spheroid sections (Fig. 6C), whereas total RPS6 levels were unchanged throughout the spheroid (Fig. S4B). Moreover, phospho-RPS6 in HCT116 cells showed the same zonal

Journal of Cell Science (2016) 0, 1-16 doi:10.1242/jcs.188102

pattern as in DLD-1 spheroids under the different treatments in 3D (Fig. 6C; Fig. S3B). Phospho-RPS6 levels were quantified by performing image analysis (Fig. 6D). Notably, the mean of all zones (Fig. 6D, red dotted lines) closely recapitulated the pattern found in western blots (Fig. S2A). Ki67 and DAPI signal intensities in the three zones were also determined. The nuclei of the cells in the spheres were evenly stained with DAPI (Fig. 6E). The proliferation marker Ki67 exhibited a well-described decrease of $Ki67^+$ cells from the outside to the core of the spheroid (Grimes et al., 2014; Laurent et al., 2013). $Ki67^+$ cells were significantly reduced in the treated samples as compared to the control (Fig. 6F; Table S3). Under treatment, $Ki67^+$ cells did not completely overlap with the strict pattern of phospho-RPS6 expression, indicating that the mTOR–S6K pathway is not solely or directly involved in the cell cycle changes of HCT116 cells grown as spheres. Taken together, our data show that the spatial differences in the activities of mTOR–S6K in human CRCs *in vivo* are faithfully reproduced in the spheroid model.

Global overview of signaling differences in 2D vs 3D culture under normal and AKT–mTOR–S6K and MAPK pathway inhibitor treatment

In order to normalize the results of this extensive study for simultaneous comparative evaluation, fold changes relative to the respective DMSO controls in the 2D and 3D systems were calculated and presented in heatmaps (Fig. 7). First, 2D vs 3D cultures were compared under normal growth conditions. The obtained data were arranged according to the mean change calculated for all cell lines (Fig. 7A). This allowed assessment and identification of responsive phenotypes or signaling molecules, and permitted general statements to be made. At first, a general significant down modulation of AKT signaling was detectable in the 3D cultures (loss of S473 and T308 phosphorylation, as well as reduced levels of phospho-PRAS40, one downstream target of AKT). Secondly, phosphorylation of S6K and RPS6 was substantially impaired in 3D cultures of all cell lines. Together with the decrease of hyperphosphorylated 4E-BP1γ, these data clearly indicate a general decrease in mTORC1 activity in the 3D system. Interestingly, phospho-ERK1/2 levels were highly variable, whereas phospho-PKC and E-cadherin expression was induced in the 3D spheroid culture. All the different responses could not be correlated to the mutational status (Fig. 7A, right).

The common and differential responses to treatment with inhibitors in 2D and 3D culture are summarized in Fig. 7B. Most obviously, S6K, RPS6 and 4EBP1 phosphorylation was efficiently blocked in 2D and 3D culture with all tested inhibitors, except for PF4708671 treatment, which resulted in S6K hyperphosphorylation both in 2D and 3D systems. It is well documented that binding of PF4708671 to S6K promotes its phosphorylation by mTORC1 but retains S6K in an inactive state (Pearce et al., 2010). All inhibitors resulted in a considerably decreased spheroid size. However, the proportion of cells in S-phase was unaltered by PF4708671 in DLD-1 cells in 3D culture, but the proportion of S-phase cells in Caco-2 both in the 2D and the 3D models was increased. Intracellular ATP levels were decreased in DLD-1 and HCT116 cells in 2D and 3D cultures, and in Caco-2 cells in 2D culture. However, treatment with rapamycin, Torin1 and AZD6244 slightly induced ATP content in Caco-2 cells in 3D culture for unknown reasons. Most interestingly, there was an increase of phospho-ERK1/2 in 2D cultures when treated with AKT, mTOR or S6K inhibitors, whereas the opposite was true for HCT116 and DLD-1 3D spheroids (Fig. 7B, bottom panel).

We identified spatial differences in RPS6 phosphorylation in spheroids under normal growth conditions. Phospho-RPS6 levels were high at the outer rim of DLD-1 and HCT116 spheroids and gradually decreased towards the inner core of the spheres. Interestingly, a similar phospho-RPS6 gradient was also detected *in vivo* in the same CRC cells grown as xenografted tumors in mice. Here, phospho-RPS6 levels were highest in close vicinity to blood vessels and diminished with increasing distance from the vessel (Fig. 7C). The phospho-RPS6 signal was almost completely abolished in rapamycin- or Torin1-treated samples, which fully blocked phospho-RPS6 in all three zones. On the contrary, phospho-RPS6 levels were reduced in each zone upon treatment with PF4708671, MK2206 or AZD6244, but the outer zone still displayed higher signals as compared to the respective middle and inner zones (Fig. 7D).

Identification of signaling pathways altered in 3D vs 2D cultures upstream of AKT–mTOR

We used phospho-receptor tyrosine kinase (phospho-RTK) arrays as a first attempt to identify potentially altered signaling pathways upstream of AKT or mTOR–S6K that might also be responsible for the decreased AKT and/or mTOR–S6K activities in 3D culture. 28 different RTKs and 11 intracellular phospho-protein signaling molecules were evaluated in DLD-1 and HCT116 cells grown in 2D or 3D culture. The global phospho-RTK profile is shown in a heatmap (Fig. 8A). As a general downregulation of AKT and mTOR–S6K activities was identified, we focused on consistently downregulated phospho-RTKs in 3D compared to 2D culture in DLD-1 and HCT116 cells. Surprisingly, we detected a consistent loss of Eph receptor (Eph; EphA2, EphA3 and EphB4) phosphorylation as well as a decrease in Src phosphorylation (Fig. 8B,C). Interestingly, ErbB2 (also known as HER2) and ErbB3 signaling was non-uniformly changed in 2D vs 3D cultures. In DLD-1 spheroids, ErbB2 and ErbB3 phosphorylation was significantly increased, whereas there was a sharp decrease of ErbB2 and ErbB3 phosphorylation in HCT116 spheroids compared to in the 2D cultures. Importantly, AKT as well as RPS6 phosphorylation was significantly reduced in the 3D system (Fig. 8C), as expected from our previous results.

DISCUSSION

The overall survival rate of individuals with cancer undergoing systemic therapy has been extended only marginally over the past 30 years. Cancer therapy for advanced cancers is far from being efficient to date (Scannell et al., 2012). Despite some key therapeutic success in targeted therapy, the current fail rate of anti-cancer compounds in clinic trials is 96% (Bhattacharjee, 2012). Clearly, there is an urgent need for more innovative pre-clinical *in vitro* models to thoroughly test promising compounds before proceeding into clinical trials.

3D models might provide better predictive power by more faithfully recapitulating the response of human tumors to anti-cancer compounds *in vivo*. This study is not a complete and comprehensive assessment of every organotypic and/or 3D model currently available (Stadler et al., 2015; Unger et al., 2014), but intentionally focuses on the comparison of 2D monolayers with free-floating 3D spheroids. This relatively simple model lacks the interaction of cancer cells with their environment, such as ECM and/or stromal cells, and has been used for long time to better mimic chemotherapeutic and radiation therapy response *in vitro*.

With regard to metastasis, the predominance and importance of single circulating tumor cells *in vivo* is well accepted. However, there is recent evidence that primary tumor cell spheroids might be also of *in vivo* relevance. Cancer cell clusters have been identified to

Journal of Cell Science (2016) 0, 1-16 doi:10.1242/jcs.188102

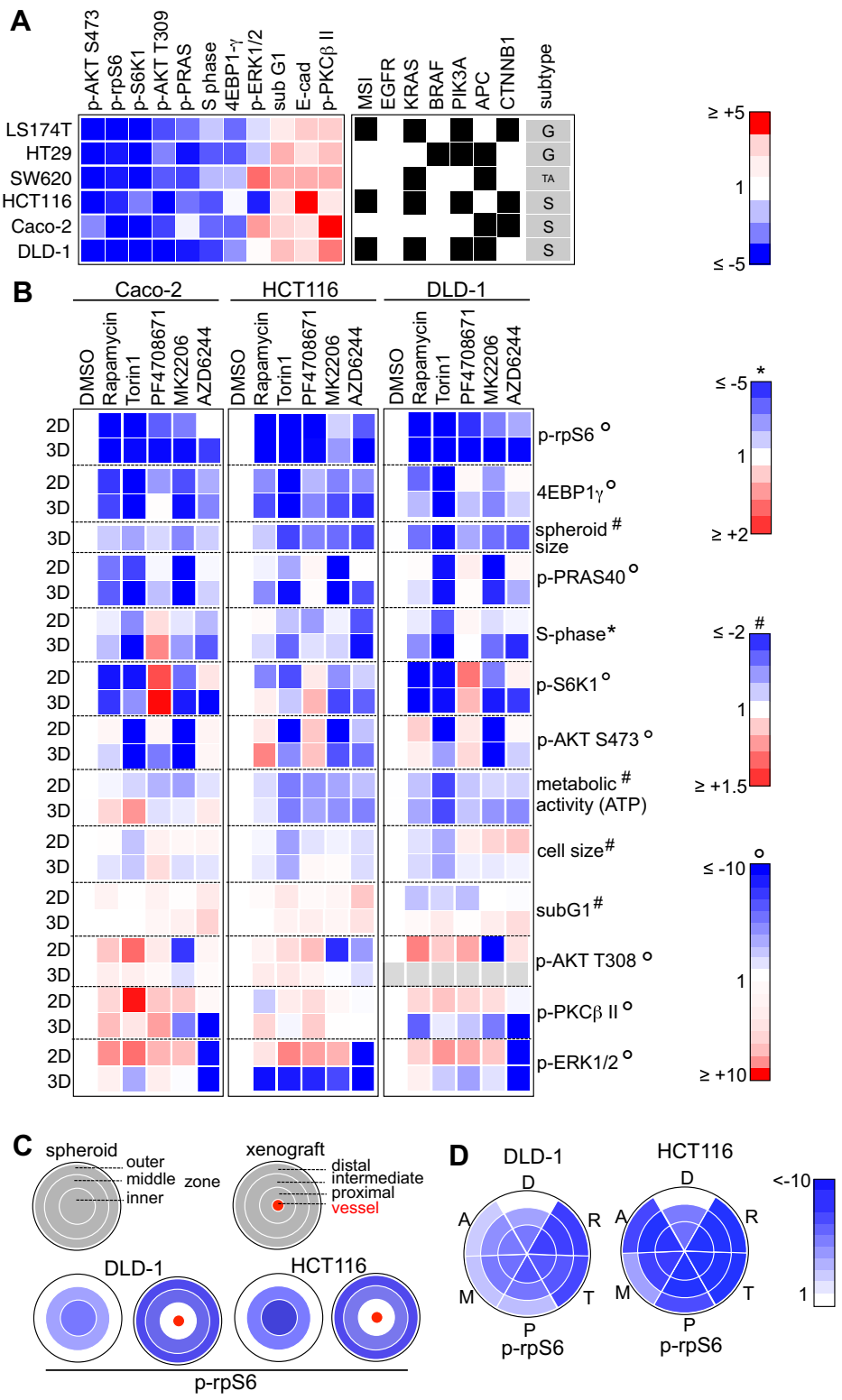

Fig. 7. Schematic overview of all results obtained in this study. Heatmaps indicate mean fold changes. Downregulation is indicated in blue, upregulation in red. (A) Regulation (fold change relative to result in 2D culture) of cell cycle distribution and of PI3K–AKT–mTOR and RAS–RAF–MAPK signaling, and an overview of mutations are given for the six colon cancer cell lines (LS174T, HT29, SW620, HCT116, Caco-2, DLD-1) in 3D compared to 2D cultures. The cancer cell transcriptional subtype is indicated: G, goblet like; TA, transit-amplifying like; S, stem-cell like. Black, mutations present; white, wild type. (B) For Caco-2, HCT116 and DLD-1 cells, differences in the regulation (fold change to respective DMSO controls) of signaling molecules, cell cycle distribution, cell size, metabolic capacity and spheroid size in 2D and 3D cell culture upon inhibition of different targets of the pathways are shown. (C) Similar regulation (fold change relative to the mean intensity of the outer zone or vessel-proximal zone) of phospho (p)-RPS6 (residues S240 and S244) in DMSO-treated DLD-1 and HCT116 spheroids (left of each pair) or in DLD-1 and HCT116 xenograft tumors (right of each pair) separated into outer, middle and inner zones, or into vessel-proximal, intermediate and distal zones, respectively. (D) Regulation (fold change relative to the mean intensity of DMSO controls) of p-RPS6 (S240 and S244) in control and treated (R, rapamycin; T, Torin1; P, PF4708671; M, MK2206; A, AZD6244) DLD-1 and HCT116 spheroids separated into outer, middle and inner zones.

pass through lymphatic endothelial cell layers in human mammary carcinomas (Kerjaschki et al., 2011), whereas colon cancer clusters have been found in blood vessels in human CRC. In CRC, two types of clusters have been identified, which differed in their polarity. On the one hand, they interacted with their environment, and on the other hand, cancer cell spheres with inverse polarity lacked contact to host structures, closely resembling *in vitro* generated spheroids. Of note, these cancer-tissue-derived spheres have also been shown to be critically involved in liver metastasis in mice (Okuyama et al., 2016). Thus, these results might qualify spheroids as proper models to recapitulate specific subsets of cancer metastasis. Nevertheless, comprehensive systematic investigations on phenotypic changes, potentially altered signaling pathways and the response to drug treatment in 2D vs 3D systems have only occasionally been performed (Ekert et al., 2014; Luca et al., 2013; Pickl and Ries, 2009). We focused on colon carcinoma, being the third most deadly

Journal of Cell Science (2016) 0, 1-16 doi:10.1242/jcs.188102

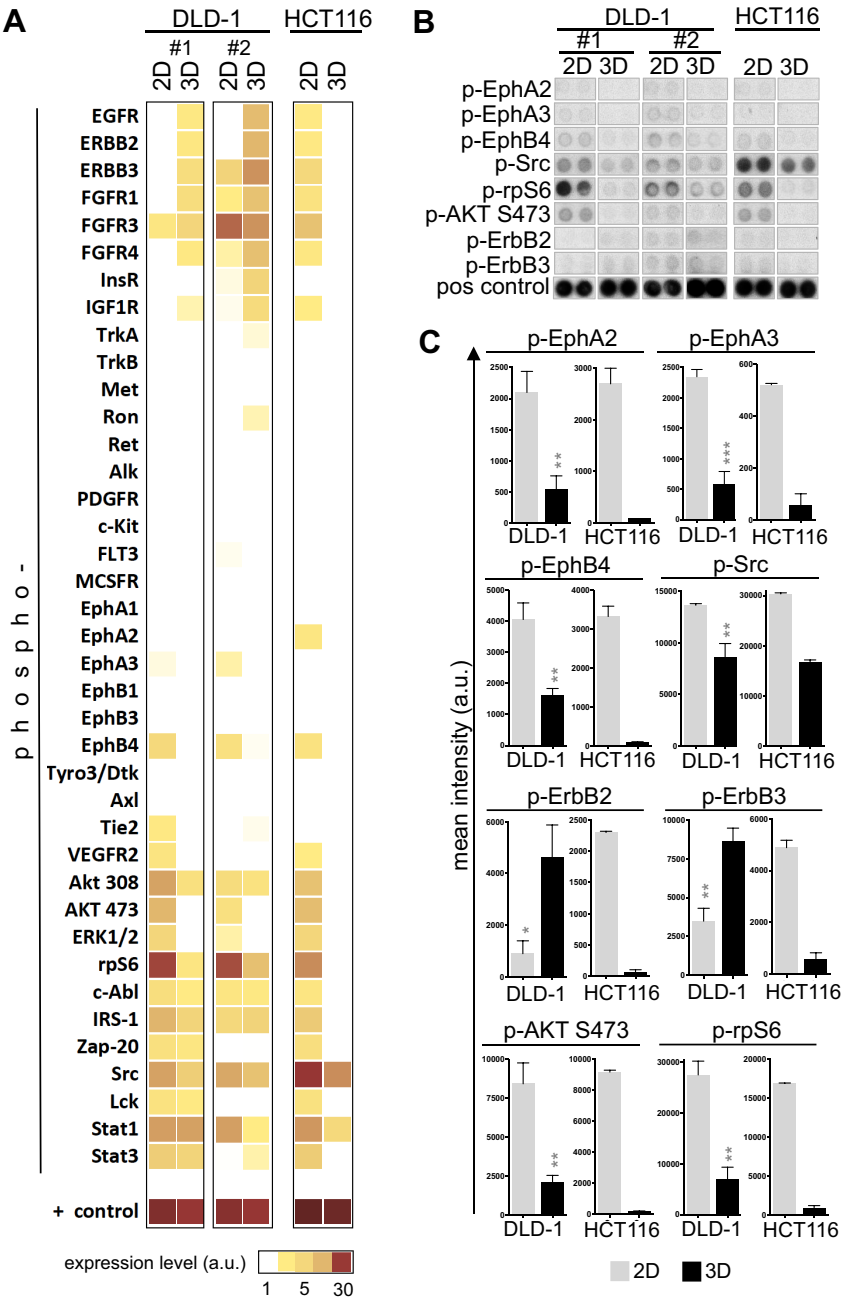

Fig. 8. Analysis of phosphorylation levels of RTKs. DLD-1 and HCT116 cells were grown as monolayers and spheroids (3000 cells/spheroid) for 48 h. 2D and 3D samples were harvested and subjected to phospho-RTK analysis using the PathScan® Array. Spot intensities were quantified by densitometry using ImageJ. (A) Heatmaps show the distinct expression levels of 18 phospho-RTKs and 11 signaling nodes in DLD-1 (two biological replicates, #1 and #2) and HCT116 cells in 2D vs 3D cultures. Absent or very low signals are indicated in white, high expression in red and intermediate signals in yellow. (B) Selected spots are shown. 'p-' prefix indicates phosphorylated protein with phosphorylated residue stated. Pos, positive. (C) Different expression patterns of particular phospho-RTKs and other signaling molecules. Bars represent means (DLD-1, n=4; HCT, n=2 replicates); error bars indicate the range. Student's t-test (unpaired, two-tailed); *$P\leq0.05$, **$P\leq0.01$, ***$P\leq0.001$.

cancer in the world, to thoroughly evaluate the main signaling pathways in 2D vs 3D spheroid cultures under normal and treated conditions.

Our findings that AKT and mTOR signaling is drastically reduced in our 3D system lead to questioning of the reasons and the underlying mechanisms. In fact, it has been shown that RTK signaling upstream of AKT–mTOR is specifically induced in 3D compared to 2D cultures. For EGFR/ErbB signaling in HER2-overexpressing breast and ovarian cancer cells, it has been shown that 3D culture results in HER2 activation in contrast to 2D culture (Pickl and Ries, 2009; Weigelt et al., 2010). Another study using lung cancer cultures has demonstrated elevated basal levels of EGFR and Met phosphorylation levels upon 3D culture compared to the levels in 2D culture (Ekert et al., 2014). Counterintuitively, activation of HER2 signaling is associated with decreased phospho-AKT levels in the breast and ovarian cancer cells. In line with this discrepancy, RTK profiling in HCT116 and DLD-1 cells revealed striking differences in EGFR signaling, showing a significant increase in ErbB2 and ErbB3 phosphorylation in DLD-1 spheroids, whereas HCT116 spheres displayed reduced phospho-ErbB2 and -ErbB3 levels as compared to the levels in 2D cultures. However, consistent with the breast cancer study, AKT signaling was decreased in both cell lines in 3D culture. In fact, all six CRC cell lines used in our study showed decreased AKT activity. Of note, reduction of AKT phosphorylation in 3D compared to 2D systems has been described in another study with CRC (Luca et al., 2013) and breast cancer cells (Weigelt et al., 2010), thus pointing to a general mechanism in 3D cultures. Interestingly, we observed loss of Eph and Src phosphorylation in 3D compared to 2D cultures of HCT116 and DLD-1 cells, as demonstrated by RTK profiling. However, phosphorylation levels of Eph were low. Importantly, these data are only correlative, and further functional experiments

Journal of Cell Science (2016) 0, 1-16 doi:10.1242/jcs.188102

are needed to decipher the impact of Ephrin–Eph signaling on AKT–mTOR activities in spheroids. One alternative explanation for the loss of AKT activation in 3D cultures is that signaling is switching from the AKT–mTOR pathway in 2D monolayers to the RAS–RAF–MAPK pathway in the 3D system. Indeed, phospho-MEK1 levels were increased in 3D cultures of breast and ovarian cancers; however, phospho-ERK1/2 levels are not substantially increased (Pickl and Ries, 2009) or have not been assessed (Weigelt et al., 2010). In colon cancers, expression profiling has revealed activation of MAPK signaling and a slight increase of phospho-ERK1/2 levels in Lovo cells in 3D cultures (Luca et al., 2013), whereas six other CRC lines displayed the opposite regulation. Indeed, in our study of ERK1/2 phosphorylation in 3D vs 2D cultures was also highly variable in the six cell lines. Some of the above-described 3D models engage laminin rich ECM (lrECM) to induce three-dimensionality, whereas others do not. Thus, the ECM adds another level of complexity (e.g. through integrin signaling) on top of the 2D vs 3D differences. Hence, further experiments are necessary to interpret decreased AKT signaling in the 3D system. Another possibility for the loss of AKT activity in 3D cultures might be simply the loss of integrin signaling, which is activated in 2D cultures by attachment to the plastic surface (or an ECM substrate) and thus induces AKT activation (Persad and Dedhar, 2003). Unfortunately, phospho-AKT levels in CRC spheroids were so low that it was not possible to detect spatial differences by performing immunofluorescence analysis. However, AKT activity might be induced through integrin signaling by embedding the spheres into ECM (basement membrane extract or collagen I gel), which is readily testable for changes in signaling in future studies by using our comprehensive approach. Alternatively, diminished AKT activity in 3D culture might be mediated through a specific increase in PTEN activity, which was not tested in this study. Notably, all six cell lines tested harbor wild-type PTEN. Nevertheless, AKT inhibitor treatment, which abolished AKT kinase activity, as demonstrated by the loss of downstream target phosphorylation, did not have such a profound effect on S6K activity in 2D as compared to 3D cultures.

To the best of our knowledge, we are the first to demonstrate that spheroid culture is associated with profoundly reduced mTORC1 signaling activity. This was revealed through diminished levels of active S6K and RPS6 phosphorylation and by the decrease of hyperphosphorylated 4E-BP1 (4E-BPγ), another target of mTORC1. Whether the reduced AKT activity is the reason for the downstream impairment of mTORC1 activity is not known. However, the decrease in phospho-RPS6 levels in 3D culture demonstrated in western blot analyses might be due to a gradual decrease of RPS6 phosphorylation in the inner regions of the spheroids, whereas in the surface area (two-cell layers), RPS6 phosphorylation remained high. This opens an alternative possibility for the diminishing mTORC1 activity inside the sphere. The inner regions of spheroids experience decreased nutrient availability (such as amino acids), which translates into diminished nutrient signaling and is mandatory for mTOR activation (Jewell et al., 2013). Indeed, intracellular amino acid concentrations rapidly drop along a gradient to the insides of spheroids (Kasinskas et al., 2014). This might explain the drastic decrease of RPS6 phosphorylation – from high levels in the outer two-cell-layer-thick zone to low levels in the deeper areas. Of note, cell proliferation also decreased gradually in the inner zones of the spheroids, as demonstrated previously (Grimes et al., 2014; Laurent et al., 2013). However, when mTOR activity was inhibited, RPS6 phosphorylation was lost but Ki67 remained, indicating that there is no direct correlation of RPS6 phosphorylation with cell proliferation. Importantly, the drop of RPS6 phosphorylation in the DLD-1 and HCT116 spheroids was also seen *in vivo* in viable cell clusters around blood vessels in tumor xenografts in mice. These results clearly qualify our spheroids as faithful models of the *in vivo* situation, at least for RPS6 phosphorylation and most probably for the upstream AKT–mTOR signaling pathway.

It is well known that the RAS–MAPK and the PI3K–AKT pathways can either positively or negatively regulate each other (Mendoza et al., 2011). Inhibition of MEK proteins can induce RTK-mediated activation of AKT through ERK-mediated inhibitory phosphorylation of GAB1 (Yu et al., 2002). On the contrary, AKT can negatively regulate ERK protein activation through inhibitory phosphorylation of RAF (Guan et al., 2000). This might explain why ERK1/2 phosphorylation was induced in all our cell lines in 2D culture upon inhibition of AKT. However, inhibiting mTOR or S6K also resulted in profound MAPK pathway activation in the 2D system. To the best of our knowledge, there are no reports on this obvious cross inhibition, which is released by AKT–mTOR pathway inhibitors. Even more puzzling is the fact that induction of ERK protein phosphorylation only occurred in 2D cultures, whereas in 3D cultures, the ERK phosphorylation was diminished upon inhibition of AKT–mTOR–S6K, suggesting a substantial rewiring of the two pathways in 3D cultures. Intriguingly, differential responses to inhibitor treatment of the three cell lines in 2D systems were abolished in 3D models, and all cell lines behaved in a similar manner, indicating a more consistent response in the 3D system.

Taken together, our results demonstrate a general theme in spheroid culture of colon cancer cells, namely the reduction in the activity of the AKT–mTOR–S6K pathway and a substantial rewiring of signaling in 3D compared to 2D culture. Our comprehensive study on colon cancer cells identifies common mechanisms that are active in 3D cultures and that are considerably different to those in 2D cultures. Despite being a simple and well-known model for many years, many unknown mechanisms are yet to be discovered in spheroids as a 3D model. Notably, the identification of sphere-like cancer cell clusters (Kerjaschki et al., 2011; Okuyama et al., 2016) entering, traveling along and escaping from vessel structures with or without interacting with the surrounding environment could result in novel perspectives for metastasis intervention. Such findings also strengthen the importance of spheroids as a valid model for mimicking certain aspects of human cancer biology. Moreover, here, we demonstrate that mTOR–S6K signaling gradients present *in vivo* are reliably reproduced in spheroid models. Thus, better understanding of 3D cancer biology *in vitro* – such as AKT–mTOR and MAPK signaling in spheroids – might aid better comprehension of cancer biology *in vivo*, prediction of the response of cancer cells to targeted therapy as well as the development of novel therapeutic concepts.

MATERIALS AND METHODS

Cell culture

Human colon cancer cell lines LS174T [American Type Culture Collection (ATCC®)#CL-188™], HT29 (ATCC®#HTB-38™), SW620 (ATCC®#CCL-227™), HCT116 (ATCC®#CCL-247™), Caco-2 (ATCC®#HTB-37™) and DLD-1 (ATCC®#CCL-221™) were obtained from the ATCC and used from early passages derived from our master cell bank. Short tandem repeat (STR) profiling was performed for cell authentication. The cells were cultivated in Dulbecco's modified Eagle's medium (DMEM) high glucose (4.5 g/l) supplemented with 10% fetal calf serum, 2 mM L-glutamine and antibiotics [60 mg/l penicillin, 100 mg/l streptomycin sulfate (PenStrep)] at 37°C under 5% CO_2.

Journal of Cell Science (2016) 0, 1-16 doi:10.1242/jcs.188102

Spheroid formation (3D culture) with 3000 cells per spheroid was induced as described (Korff and Augustin, 1998; Walzl et al., 2014). In brief, cells were detached, counted and seeded in 100 µl of DMEM with 5% FCS, glutamine and PenStrep containing 0.3% methylcellulose into 96-well plates (round bottomed, untreated) for 24 h. In parallel, cells were seeded on cell culture plates (2D culture) and cultivated in the same medium. Cells were cultured at 80% humidity, under 5% CO_2 and 20% O_2 (Walzl et al., 2012). Cultures were treated with different inhibitors for an additional 24 h. Spheroid formation time and/or the presence of methylcellulose did not alter drug response (supporting figures 8 and 9, respectively). Cellular and spheroid morphology was evaluated microscopically and was analyzed (Cell^F, Olympus, Tokyo, Japan) to determine spheroid volume by measuring projected areas, followed by radius and volume (µm³) determination.

Inhibitor treatment

For inhibitor treatment in 2D and 3D cultures, 100 nM of rapamycin (Grabiner et al., 2014; Kang et al., 2013; Sarbassov et al., 2006), 250 nM of Torin1 (Cheng et al., 2016; Grabiner et al., 2014; Kang et al., 2013; Thoreen et al., 2012), 10 µM of PF47068671 (Pearce et al., 2010; Schipany et al., 2015; Zhang et al., 2015), 1 µM of MK2206 (Devery et al., 2015; Shen et al., 2015; Sung et al., 2016) and 1 µM of AZD6244 (Devery et al., 2015; Ewald et al., 2015) were employed as these concentrations have been most frequently used in cell-based assays and have a complete effect on their respective targets [phospho-protein analysis in western blots (see Fig. 4 and western blots in the supporting figures)].

Cell cycle, cell size and metabolic activity assays

Cell cycle analysis was performed with the Click-iT® EdU Alexa Fluor® 488 Kit (Invitrogen, Thermo Scientific). Cells and spheroids were exposed to EdU (5-ethynyl-2′-deoxyuridine, 10 µM) at 37°C for 20 min. Thereafter, spheroids were trypsinized and cells were analyzed. 7-aminoactinomycin D (7AAD) was used to stain total DNA and set the forward scatter to determine cell size. The metabolic capacity of cells was determined with CellTiter-Glo® (Promega) according to the manufacturer's protocol and luminescence measurement (Synergy HT, Biotek®).

Immunoblot analysis

Whole-cell lysates were prepared from 2D or 3D cultures. Cells and spheroids were washed in PBS and extracted in RIPA lysis buffer (50 mM Tris-HCl pH 7.6, 150 mM NaCl, 1% TritonX-100, 0.1% SDS, 0.5% sodium deoxycholate, 1 mM PMSF, 4 µg/ml aprotinin, 4 µg/ml leupeptin, 0.6 µg/ml benzamidinchloride, 20 µg/ml trypsin inhibitor). Supernatants were collected after centrifugation (18,800 ***g*** at 4°C for 20 min). Equal amounts of protein (10–15 µg) were mixed with loading dye (200 mM Tris-HCl pH 6.8, 400 mM DTT, 8% SDS, 0.4% bromophenol blue, 40% glycerol), denatured, subjected to SDS-PAGE and transferred to nitrocellulose membranes. Blocked membranes were probed with primary antibodies at 4°C overnight and with horseradish-peroxidase (HRP)-conjugated secondary antibodies (anti-mouse-IgG heavy and light chain, and anti-rabbit-IgG heavy and light chain, Bethyl Laboratories) at room temperature for 1 h. Signals were detected using chemiluminescence and X-ray films. The mean integrated density of each band was determined with ImageJ (National Institutes of Health). For antibodies, see Table S2.

Immunohistochemistry and immunofluorescence

Cells and spheroids were fixed in 4% paraformaldehyde (PFA) at room temperature for 30 min. Fixed spheroids were molded into agarose gels (1%), embedded into paraffin, sectioned (5 µm) and subjected for antigen retrieval in citrate buffer pH 6 (DAKO) at 120°C for 10 min.

For immunohistochemical staining, endogenous peroxidase activity was blocked in 3% H_2O_2 for 10 min. Blocking was performed in horse serum (2.5% in PBS, Vector Laboratories) for 20 min at room temperature. Primary antibody incubation was performed at 4°C overnight and secondary antibody (biotin labeled, Vector Laboratories) was performed at room temperature for 1 h, followed by streptavidin–HRP (Leica Microsystems, Germany) incubation for 30 min at 4°C and chromogenic development (AEC, DAKO). Nuclei were counterstained with hematoxylin, and slides were coverslipped (Aquatex®, Merck-Millipore). 20× (3D) and 40× (2D) objectives (NA=1.3) were used.

For immunofluorescence, spheroids were handled as described above. In 2D culture, cells fixed in PFA (4%) were permeabilized in methanol at −20°C for 10 min. 2D and 3D culture samples were blocked in PBS with 1% BSA at room temperature for 1 h. Primary antibody incubation was performed at 4°C overnight. Alexa-Fluor®488- and Alexa-Fluor®546-conjugated secondary antibodies (Thermo Scientific) were used at room temperature for 1 h. Nuclei were counterstained with 2 µg/ml DAPI (Sigma). Slides were mounted with Vectashield® (Vector Laboratories). Confocal fluorescence images were recorded on a Leica-SP8 with a 20× immersion objective (NA=1.3).

Automated spheroid zonation and image analysis

Image analysis of spheroid sections was performed with StrataQuest software (TissueGnostics, Vienna, Austria). For automated spheroid detection, a virtual channel was created followed by threshold segmentation, generation of a background mask followed by distance transformation. Three intervals were set on this distance-transformed image to correspond to three zones of interest in the spheroid. The outer zone was set to be two-cell-layer thick; the remaining zones were equally divided. Nuclear detection was performed in the DAPI channel, and cellular masks were computed. For each cell, the intensities for the DAPI, phospho-RPS6 and Ki67 channels were calculated and assigned to a certain zone. For quantification of phospho-RPS6 in the areas around cross-sectioned blood vessels in HCT116 and DLD-1 xenografted tumors, the same image analysis was performed except that the zonation was performed by hand. The vessel-proximal zone was defined by a three-cell-layer thickness immediately around the vessel, followed by an intermediate and a vessel-proximal area of similar size to the analyzed spheroids.

RTK signaling antibody array

Phosphorylation levels of RTKs and other signaling nodes were determined (Cell Signaling Technology). DLD-1 and HCT116 colon cancer cells cultivated in 2D and 3D cultures in normal growth medium (DMEM, 5% FCS) were harvested 48 h after seeding. The assay was performed as described in the manufacturer's protocol. The arrays were developed using X-ray films; spot intensities were quantified and the background was corrected using ImageJ.

Statistical analysis

Bar graphs are presented as mean±s.d. or s.e.m. For statistical analysis, Student's *t*-test (unpaired, two-tailed) was performed. *P*-values are indicated as $*P \leq 0.05$, $**P \leq 0.01$, $***P \leq 0.001$ or $****P \leq 0.0001$. For exact *P*-values of all experiments, see Table S3.

Acknowledgements

We thank Dr Julia Schüler (Oncotest, Freiburg, Germany) for xenograft tumors and Eduard Clim (TissueGnostics Vienna) for help with StrataQuest. Some of this work is also presented in the thesis of Angelika Riedl (2017, Evaluating PI3K/AKT/mTOR and MAPK signaling in 3D colon cancer models to identify effective combination therapy approaches, Medical University of Vienna).

Competing interests

The authors declare no competing or financial interests.

Author contributions

A.R. and H.D. designed the research; A.R., M. Schlederer, K.P., M. Stadler, S.W., D.U., C.U., N.K. performed the research; A.R. and H.D. analyzed the data; D.P., L.K., M.H., G.K. were involved in manuscript preparation; A.R. and H.D. wrote the manuscript; all authors approved the manuscript for publication.

Funding

This work was supported by the Niederösterreichische Forschungs- und Bildungsges.m.b.H (NFB). A.R. was a recipient of a DOC fellowship from the Austrian Academy of Sciences (ÖAW).

Data availability

Supporting figures are available at figshare https://figshare.com/s/c80fdda565dc5e338f42 (doi: 10.6084/m9.figshare.3470273).

Supplementary information

Supplementary information available online at
http://jcs.biologists.org/lookup/doi/10.1242/jcs.188102.supplemental

References

Bhattacharjee, Y. (2012). Biomedicine. Pharma firms push for sharing of cancer trial data. *Science* **338**, 29.

Bodnar, A. G., Ouellette, M., Frolkis, M., Holt, S. E., Chiu, C.-P., Morin, G. B., Harley, C. B., Shay, J. W., Lichtsteiner, S. and Wright, W. E. (1998). Extension of life-span by introduction of telomerase into normal human cells. *Science* **279**, 349-352.

Cheng, N.-T., Guo, A. and Meng, H. (2016). The protective role of autophagy in experimental osteoarthritis, and the therapeutic effects of Torin 1 on osteoarthritis by activating autophagy. *BMC Musculoskelet. Disord.* **17**, 150.

Desoize, B. and Jardillier, J.-C. (2000). Multicellular resistance: a paradigm for clinical resistance? *Crit. Rev. Oncol. Hematol.* **36**, 193-207.

Devery, A. M., Wadekar, R., Bokobza, S. M., Weber, A. M., Jiang, Y. and Ryan, A. J. (2015). Vascular endothelial growth factor directly stimulates tumour cell proliferation in non-small cell lung cancer. *Int. J. Oncol.* **47**, 849-856.

Dolznig, H., Rupp, C., Puri, C., Haslinger, C., Schweifer, N., Wieser, E., Kerjaschki, D. and Garin-Chesa, P. (2011). Modeling colon adenocarcinomas in vitro a 3D co-culture system induces cancer-relevant pathways upon tumor cell and stromal fibroblast interaction. *Am. J. Pathol.* **179**, 487-501.

Ekert, J. E., Johnson, K., Strake, B., Pardinas, J., Jarantow, S., Perkinson, R. and Colter, D. C. (2014). Three-dimensional lung tumor microenvironment modulates therapeutic compound responsiveness in vitro–implication for drug development. *PLoS ONE* **9**, e92248.

Ewald, F., Nörz, D., Grottke, A., Bach, J., Herzberger, C., Hofmann, B. T., Nashan, B. and Jücker, M. (2015). Vertical targeting of AKT and mTOR as well as dual targeting of AKT and MEK signaling is synergistic in hepatocellular carcinoma. *J. Cancer* **6**, 1195-1205.

Fingar, D. C., Salama, S., Tsou, C., Harlow, E. and Blenis, J. (2002). Mammalian cell size is controlled by mTOR and its downstream targets S6K1 and 4EBP1/eIF4E. *Genes Dev.* **16**, 1472-1487.

Fischbach, C., Kong, H. J., Hsiong, S. X., Evangelista, M. B., Yuen, W. and Mooney, D. J. (2009). Cancer cell angiogenic capability is regulated by 3D culture and integrin engagement. *Proc. Natl. Acad. Sci. USA* **106**, 399-404.

Grabiner, B. C., Nardi, V., Birsoy, K., Possemato, R., Shen, K., Sinha, S., Jordan, A., Beck, A. H. and Sabatini, D. M. (2014). A diverse array of cancer-associated MTOR mutations are hyperactivating and can predict rapamycin sensitivity. *Cancer Discov.* **4**, 554-563.

Grimes, D. R., Kelly, C., Bloch, K. and Partridge, M. (2014). A method for estimating the oxygen consumption rate in multicellular tumour spheroids. *J. R. Soc. Interface* **11**, 20131124.

Guan, K.-L., Figueroa, C., Brtva, T. R., Zhu, T., Taylor, J., Barber, T. D. and Vojtek, A. B. (2000). Negative regulation of the serine/threonine kinase B-Raf by Akt. *J. Biol. Chem.* **275**, 27354-27359.

Hahn, W. C., Counter, C. M., Lundberg, A. S., Beijersbergen, R. L., Brooks, M. W. and Weinberg, R. A. (1999). Creation of human tumour cells with defined genetic elements. *Nature* **400**, 464-468.

Hidalgo, I. J., Raub, T. J. and Borchardt, R. T. (1989). Characterization of the human colon carcinoma cell line (Caco-2) as a model system for intestinal epithelial permeability. *Gastroenterology* **96**, 736-749.

Hirschhaeuser, F., Menne, H., Dittfeld, C., West, J., Mueller-Klieser, W. and Kunz-Schughart, L. A. (2010). Multicellular tumor spheroids: an underestimated tool is catching up again. *J. Biotechnol.* **148**, 3-15.

Iyer, V. R., Eisen, M. B., Ross, D. T., Schuler, G., Moore, T., Lee, J. C. F., Trent, J. M., Staudt, L. M., Hudson, J., Jr, Boguski, M. S. et al. (1999). The transcriptional program in the response of human fibroblasts to serum. *Science* **283**, 83-87.

Jewell, J. L., Russell, R. C. and Guan, K.-L. (2013). Amino acid signalling upstream of mTOR. *Nat. Rev. Mol. Cell Biol.* **14**, 133-139.

Kang, S. A., Pacold, M. E., Cervantes, C. L., Lim, D., Lou, H. J., Ottina, K., Gray, N. S., Turk, B. E., Yaffe, M. B. and Sabatini, D. M. (2013). mTORC1 phosphorylation sites encode their sensitivity to starvation and rapamycin. *Science* **341**, 1236566.

Kasinskas, R. W., Venkatasubramanian, R. and Forbes, N. S. (2014). Rapid uptake of glucose and lactate, and not hypoxia, induces apoptosis in three-dimensional tumor tissue culture. *Integr. Biol.* **6**, 399-410.

Kerjaschki, D., Bago-Horvath, Z., Rudas, M., Sexl, V., Schneckenleithner, C., Wolbank, S., Bartel, G., Krieger, S., Kalt, R., Hantusch, B. et al. (2011). Lipoxygenase mediates invasion of intrametastatic lymphatic vessels and propagates lymph node metastasis of human mammary carcinoma xenografts in mouse. *J. Clin. Invest.* **121**, 2000-2012.

Korff, T. and Augustin, H. G. (1998). Integration of endothelial cells in multicellular spheroids prevents apoptosis and induces differentiation. *J. Cell Biol.* **143**, 1341-1352.

Laplante, M. and Sabatini, D. M. (2012). mTOR signaling in growth control and disease. *Cell* **149**, 274-293.

Laurent, J., Frongia, C., Cazales, M., Mondesert, O., Ducommun, B. and Lobjois, V. (2013). Multicellular tumor spheroid models to explore cell cycle checkpoints in 3D. *BMC Cancer* **13**, 73.

Luca, A. C., Mersch, S., Deenen, R., Schmidt, S., Messner, I., Schäfer, K.-L., Baldus, S. E., Huckenbeck, W., Piekorz, R. P., Knoefel, W. T. et al. (2013). Impact of the 3D microenvironment on phenotype, gene expression, and EGFR inhibition of colorectal cancer cell lines. *PLoS ONE* **8**, e59689.

Marisa, L., de Reyniès, A., Duval, A., Selves, J., Gaub, M. P., Vescovo, L., Etienne-Grimaldi, M.-C., Schiappa, R., Guenot, D., Ayadi, M. et al. (2013). Gene expression classification of colon cancer into molecular subtypes: characterization, validation, and prognostic value. *PLoS Med.* **10**, e1001453.

Medico, E., Russo, M., Picco, G., Cancelliere, C., Valtorta, E., Corti, G., Buscarino, M., Isella, C., Lamba, S., Martinoglio, B. et al. (2015). The molecular landscape of colorectal cancer cell lines unveils clinically actionable kinase targets. *Nat. Commun.* **6**, 7002.

Mendoza, M. C., Er, E. E. and Blenis, J. (2011). The Ras-ERK and PI3K-mTOR pathways: cross-talk and compensation. *Trends Biochem. Sci.* **36**, 320-328.

Okawa, T., Michaylira, C. Z., Kalabis, J., Stairs, D. B., Nakagawa, H., Andl, C. D., Johnstone, C. N., Klein-Szanto, A. J., El-Deiry, W. S., Cukierman, E. et al. (2007). The functional interplay between EGFR overexpression, hTERT activation, and p53 mutation in esophageal epithelial cells with activation of stromal fibroblasts induces tumor development, invasion, and differentiation. *Genes Dev.* **21**, 2788-2803.

Okuyama, H., Kondo, J., Sato, Y., Endo, H., Nakajima, A., Piulats, J. M., Tomita, Y., Fujiwara, T., Itoh, Y., Mizoguchi, A. et al. (2016). Dynamic change of polarity in primary cultured spheroids of human colorectal adenocarcinoma and its role in metastasis. *Am. J. Pathol.* **186**, 899-911.

Pearce, L. R., Alton, G. R., Richter, D. T., Kath, J. C., Lingardo, L., Chapman, J., Hwang, C. and Alessi, D. R. (2010). Characterization of PF-4708671, a novel and highly specific inhibitor of p70 ribosomal S6 kinase (S6K1). *Biochem. J.* **431**, 245-255.

Persad, S. and Dedhar, S. (2003). The role of integrin-linked kinase (ILK) in cancer progression. *Cancer Metastasis Rev.* **22**, 375-384.

Pickl, M. and Ries, C. H. (2009). Comparison of 3D and 2D tumor models reveals enhanced HER2 activation in 3D associated with an increased response to trastuzumab. *Oncogene* **28**, 461-468.

Pinto, M., Robine-Leon, S., Appay, M. D., Kedinger, M., Triadou, N., Dussaulx, E., Lacroix, B., Simon-Assman, P., Haffen, K., Fogh, J. et al. (1983). Enterocyte-like differentiation and polarization of the human colon carcinoma cell line Caco-2 in culture. *Biol. Cell* **47**, 323-330.

Sarbassov, D. D., Ali, S. M., Sengupta, S., Sheen, J.-H., Hsu, P. P., Bagley, A. F., Markhard, A. L. and Sabatini, D. M. (2006). Prolonged rapamycin treatment inhibits mTORC2 assembly and Akt/PKB. *Mol. Cell* **22**, 159-168.

Scannell, J. W., Blanckley, A., Boldon, H. and Warrington, B. (2012). Diagnosing the decline in pharmaceutical R&D efficiency. *Nat. Rev. Drug Discov.* **11**, 191-200.

Schipany, K., Rosner, M., Ionce, L., Hengstschläger, M. and Kovacic, B. (2015). eIF3 controls cell size independently of S6K1-activity. *Oncotarget* **6**, 24361-24375.

Schlederer, M., Mueller, K. M., Haybaeck, J., Heider, S., Huttary, N., Rosner, M., Hengstschläger, M., Moriggl, R., Dolznig, H. and Kenner, L. (2014). Reliable quantification of protein expression and cellular localization in histological sections. *PLoS ONE* **9**, e100822.

Shen, C., Cai, G. Q., Peng, J.-P. and Chen, X.-D. (2015). Autophagy protects chondrocytes from glucocorticoids-induced apoptosis via ROS/Akt/FOXO3 signaling. *Osteoarthritis Cartilage* **23**, 2279-2287.

Stadler, M., Walter, S., Walzl, A., Kramer, N., Unger, C., Scherzer, M., Unterleuthner, D., Hengstschläger, M., Krupitza, G. and Dolznig, H. (2015). Increased complexity in carcinomas: analyzing and modeling the interaction of human cancer cells with their microenvironment. *Semin. Cancer Biol.* **35**, 107-124.

Sung, P. L., Jan, Y. H., Lin, S. C., Huang, C. C., Lin, H., Wen, K. C., Chao, K. C., Lai, C. R., Wang, P. H., Chuang, C. M. et al. (2016). Periostin in tumor microenvironment is associated with poor prognosis and platinum resistance in epithelial ovarian carcinoma. *Oncotarget* **7**, 4036-4047.

Takagi, A., Watanabe, M., Ishii, Y., Morita, J., Hirokawa, Y., Matsuzaki, T. and Shiraishi, T. (2007). Three-dimensional cellular spheroid formation provides human prostate tumor cells with tissue-like features. *Anticancer Res.* **27**, 45-53.

Thoreen, C. C., Chantranupong, L., Keys, H. R., Wang, T., Gray, N. S. and Sabatini, D. M. (2012). A unifying model for mTORC1-mediated regulation of mRNA translation. *Nature* **485**, 109-113.

Tremblay, F., Brule, S., Hee Um, S., Li, Y., Masuda, K., Roden, M., Sun, X. J., Krebs, M., Polakiewicz, R. D., Thomas, G. et al. (2007). Identification of IRS-1 Ser-1101 as a target of S6K1 in nutrient- and obesity-induced insulin resistance. *Proc. Natl. Acad. Sci. USA* **104**, 14056-14061.

Unger, C., Kramer, N., Walzl, A., Scherzer, M., Hengstschläger, M. and Dolznig, H. (2014). Modeling human carcinomas: physiologically relevant 3D models to improve anti-cancer drug development. *Adv. Drug Deliv. Rev.* **79-80**, 50-67.

Walzl, A., Kramer, N., Mazza, G., Rosner, M., Falkenhagen, D., Hengstschlager, M., Schwanzer-Pfeiffer, D. and Dolznig, H. (2012). A simple and cost efficient

method to avoid unequal evaporation in cellular screening assays, which restores cellular metabolic activity. *Intl. J. Appl. Sci. Technol.* **2**, 17-21.

Walzl, A., Unger, C., Kramer, N., Unterleuthner, D., Scherzer, M., Hengstschlager, M., Schwanzer-Pfeiffer, D. and Dolznig, H. (2014). The resazurin reduction assay can distinguish cytotoxic from cytostatic compounds in spheroid screening assays. *J. Biomol. Screen.* **19**, 1047-1059.

Weigelt, B., Lo, A. T., Park, C. C., Gray, J. W. and Bissell, M. J. (2010). HER2 signaling pathway activation and response of breast cancer cells to HER2-targeting agents is dependent strongly on the 3D microenvironment. *Breast Cancer Res. Treat.* **122**, 35-43.

Yu, C. F., Liu, Z. X. and Cantley, L. G. (2002). ERK negatively regulates the epidermal growth factor-mediated interaction of Gab1 and the phosphatidylinositol 3-kinase. *J. Biol. Chem.* **277**, 19382-19388.

Zhang, Y., Wang, Q., Chen, L. and Yang, H.-S. (2015). Inhibition of p70S6K1 activation by Pdcd4 overcomes the resistance to an IGF-1R/IR inhibitor in colon carcinoma cells. *Mol. Cancer Ther.* **14**, 799-809.

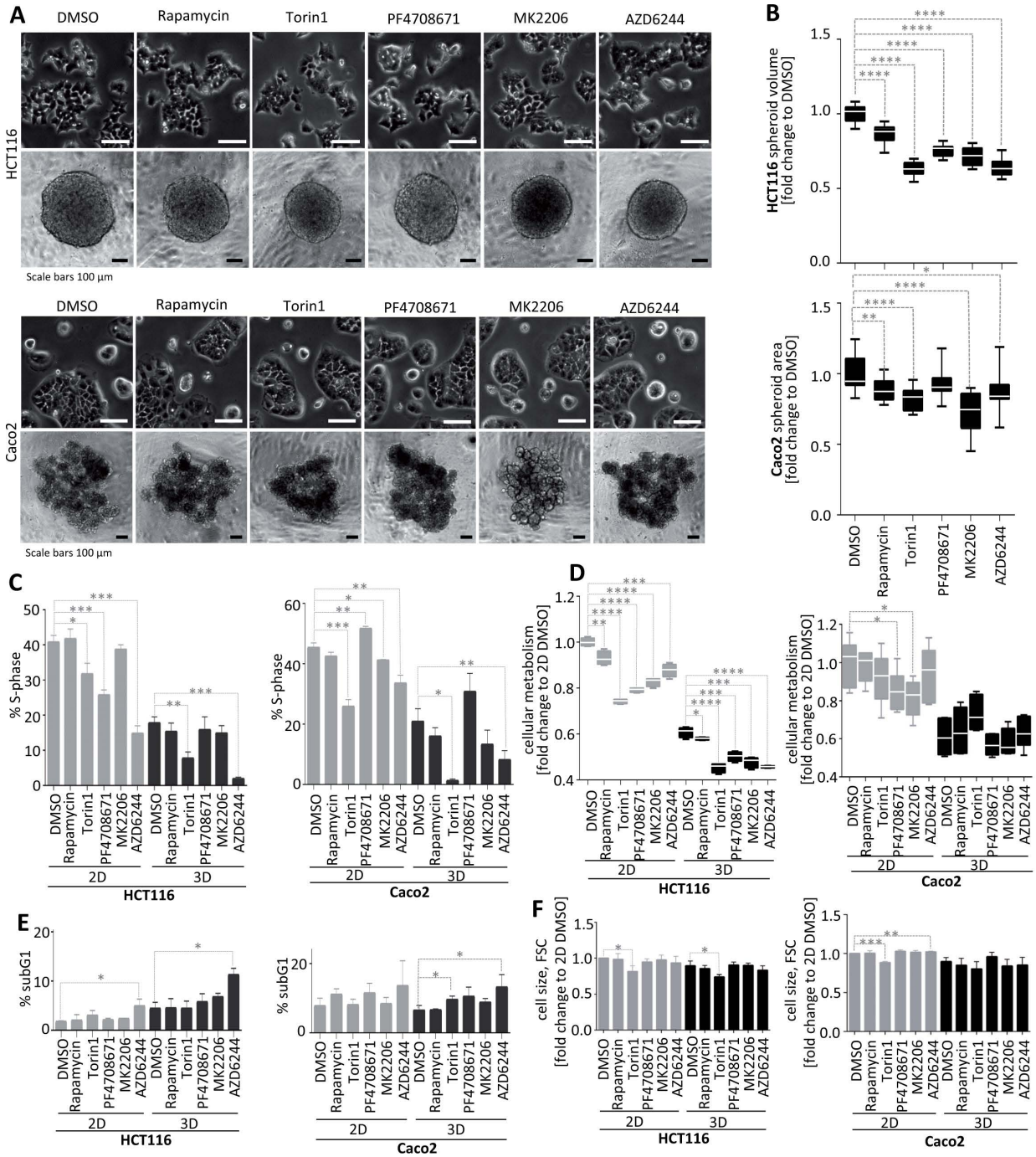

Supplementary Figure S1 – Morphologic and phenotypic analysis of colon cancer spheroids compared to monolayer cultures. HCT116 and Caco2 were grown in 2D and 3D for 24h and treated with Rapamycin (100 nM), the mTOR inhibitor Torin1 (250 nM), the S6K1 inhibitor PF4708671 (10 µM), the AKT inhibitor MK2206 (1 µM) and the MEK1 inhibitor AZD6244 (1 µM) for another 24h. DMSO served as control. Representative brightfield microscopic images of HCT116 and Caco2 (**A**) are shown. Scale bars represent 100 µm. For HCT116 (n=15 per condition) and Caco2 (n=15 per condition), the spheroid volume and the spheroid area (**B**), respectively, were calculated. The percentage of HCT116 and Caco2 in 2D and 3D cultures in S-phase (**C**) and subG1-phase (**E**) was determined using the Click-iT® EdU Alexa Fluor® 488 Flow Cytometry Assay Kit (Invitrogen, Thermo Scientific Inc., Waltham, MA). Metabolic activity (**D**) of HCT116 and Caco2 cells cultured as monolayers and spheroids ± inhibitors was evaluated using the CellTiter-Glo luminescence assay (Promega, Madison, WI) by analyzing the level of ATP present within the cells (n = 6 per condition). Evaluation of the forward scatter (FSC) was used for determining cell size of HCT116 and Caco2 (**F**) 2D and 3D cultures. Bar graphs represent the mean ± standard deviation (SD). Boxplots were created in GraphPad Prism 4. The box represents the middle 50% of the data ranging from the lower quartile (Q1) to the upper quartile (Q3). The line within the box indicates the median (Q2) and the whiskers represent the lower and upper 25% of the data - the minimum and maximum values respectively. Detailed data are available in supporting figure 2.

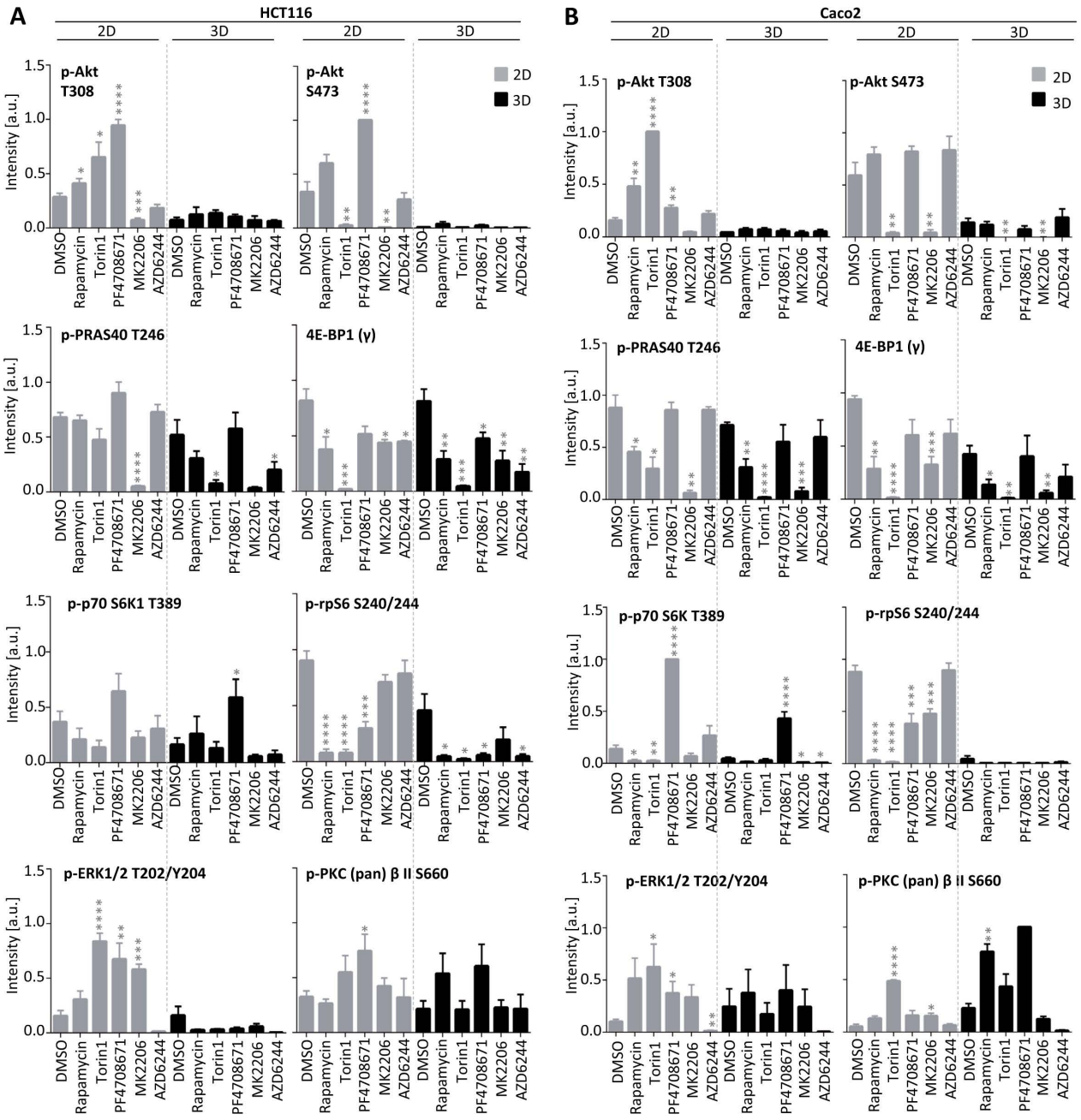

Supplementary Figure S2 – PI3K/AKT/mTOR- and RAS/RAF/MAPK-signaling in the presence or absence of inhibitory compounds. HCT116 and Caco2 colon cancer cells, grown in untreated conditions in 2D and 3D (3,000 cells per spheroid) for 24h, were treated with DMSO, 100 nM Rapamycin, 250 nM Torin1, 10 µM PF4708671, 1 µM MK2206 and 1 µM AZD6244 for another 24h. 2D and 3D cultures were harvested and subjected to Western blot analysis. The bands in Western blots from two or three independent experiments were evaluated densitometrically with ImageJ (n=2-8 per condition). Quantification is shown for (**A**) HCT116 and (**B**) for Caco2 cells. Bars are mean integrated density ±SEM. For statistical analysis Student's t-test (unpaired, two-tailed**)** was performed. p-values are indicated. Detection of phospho-proteins is indicated by a prefixed "p-". α-tubulin and GAPDH served as loading control. Western blots used for this quantification can be viewed in Supporting Figure SF5 for HCT116 and in Supporting Figure SF6 on fig**share**.

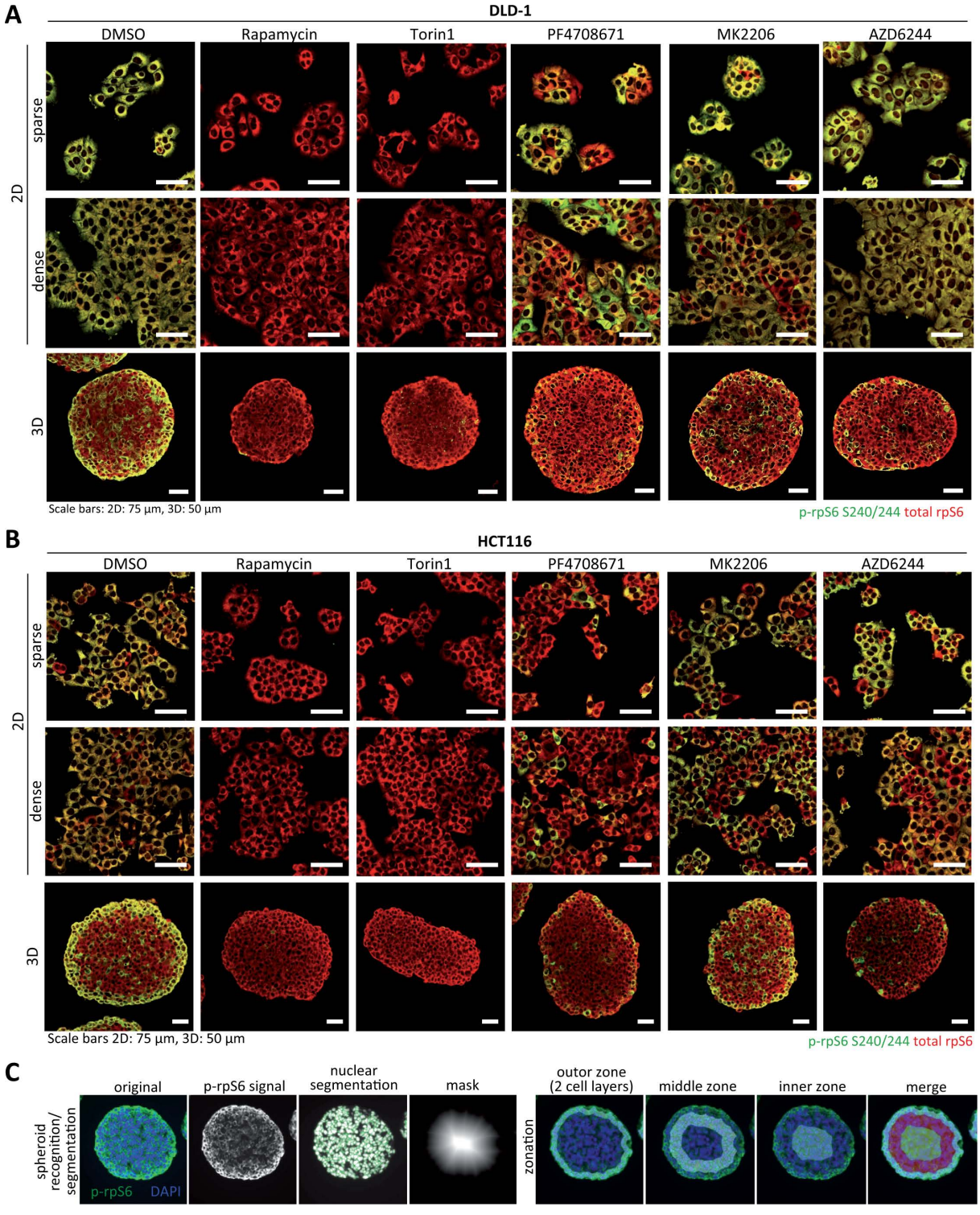

Supplementary Figure S3 – Phopsho-rpS6 and total rpS6 expression in human colon cancer spheroids. **A** DLD-1 and **B** HCT116 colon cancer cell spheroids were formed for 24h and subsequently treated with DMSO, 100 nM Rapamycin, 250 nM Torin1, 10 µM PF4708671, 1 µM MK2206 and 1 µM AZD6244 for another 24h. Spheroids were subjected to FFPE and sections stained with antibodies against phospho-rpS6 (green) and total rpS6 (red). Representative samples are shown. **C** StrataQuest software was used for automated spheroid recognition and subsequent zonation by generating a mask followed by distance transformation. This allowed automatic generation of three zones. Nuclear segmentation was performed to measure cytoplasmic p-rpS6 fluorescence intensity around individual DAPI stained nuclei in the different zones.

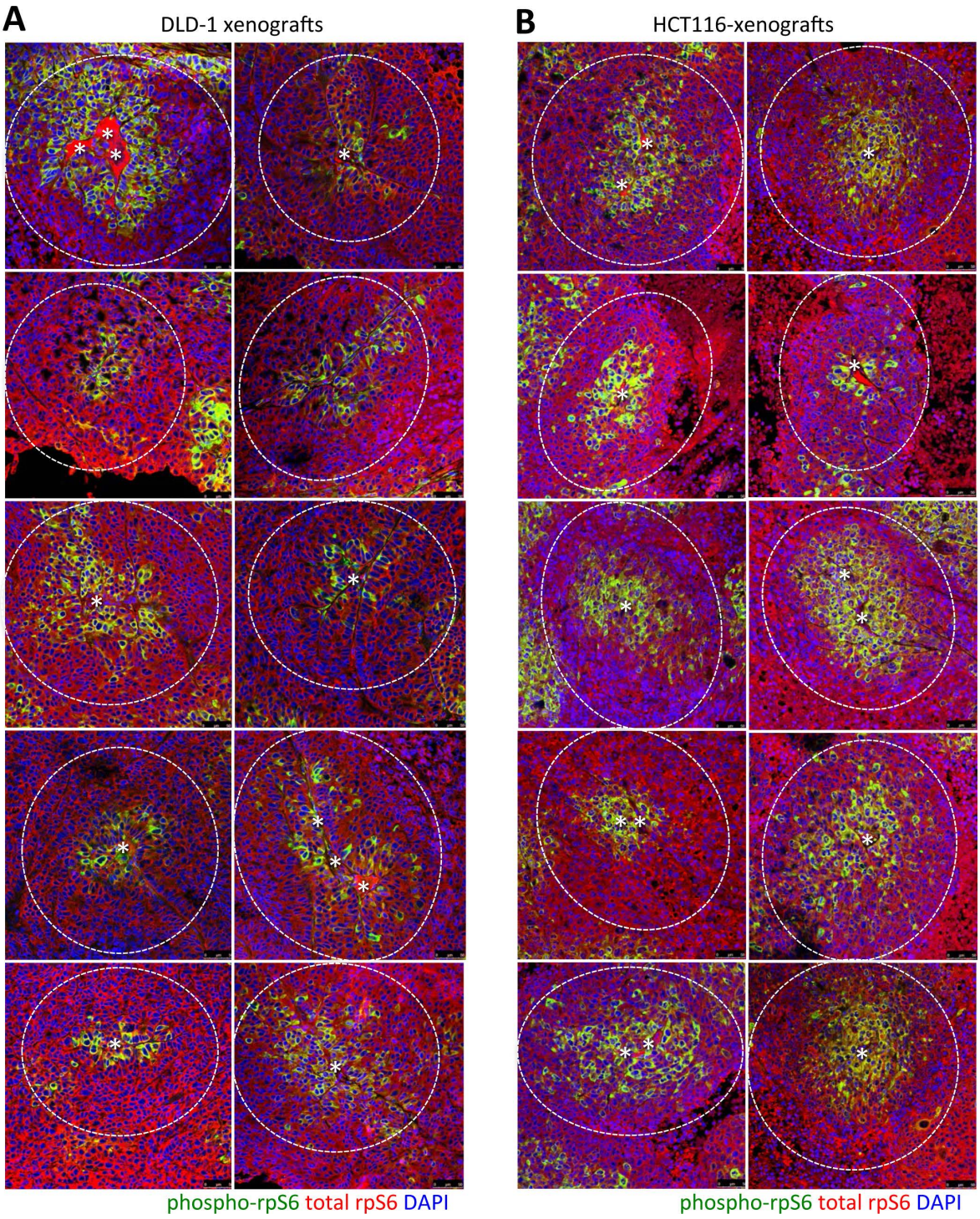

Supplementary Figure S4 – Phopsho-rpS6 and total rpS6 expression in human colon cancer xenografts.
A DLD-1 and **B** HCT116 colon cancer cells were subcutaneously injected into SCID mice and xenograft tumors were removed after reaching a size of 1cm diameter. Tumors were subjected to FFPE and sections stained with antibodies against phospho-rpS6 (green) and total rpS6 (red). Nuclei are counterstained with DAPI (blue). Analyzed areas for phopsho-rpS6 intensity quantification are shown (white dotted circles). The position of cut blood vessels perpendicular to the section plane are indicated (white stars). Scale bars (black): 50 µm.

Riedl et al

Supporting Figure legends for Figures on figshare

(https://figshare.com/s/c80fdda565dc5e338f42)

Supporting Figure SF1 (figshare) - Analysis of PI3K/AKT/mTOR- and RAS/RAF/MAPK-singaling in 2D vs 3D cell culture. The colon cancer cells (LS174T, HT29, SW620, HCT116, Caco2 and DLD-1) were cultured in 2D and 3D for 48h. Cells and spheroids were harvested and Western blot analysis of different proteins of the PI3K/AKT/mTOR- and RAS/RAF/MAPK-pathway was carried out. Detection of phosphorylated proteins is indicated by p- prior to the protein name and the phosphorylated amino acid is indicated behind the protein name. α-tubulin and GAPDH served as loading control. Two independent biological replicates are shown (**AB**).

Supporting Figure SF2 (figshare) - Analysis of cell cycle and PI3K/AKT/mTOR- and RAS/RAF/MAPK-signaling in 2D vs 3D cell culture. The colon cancer cells (LS174T, HT29, SW620, HCT116, Caco2 and DLD-1) were cultured in 2D and 3D for 48h. Cells and spheroids were harvested and cell cycle analysis (**A**) was performed using the Click-iT® EdU Alexa Fluor® 488 Flow Cytometry Assay Kit (Invitrogen, Thermo Scientific Inc., Waltham, MA) (LS174T: n = 4, HT29: n = 3, SW620: n = 6, HCT116: n = 8, Caco2: n = 4, DLD-1: n = 9 per condition).

Supporting Figure SF3 (figshare) - Apoptosis detection in HCT116 cells to inhibitor treatment in 2D vs 3D. HCT116 cells were grown as monolayer and spheroids (3,000 cells per spheroid) for 24h. 2D and 3D samples were cultured in the presence or absence of Rapamycin, Torin1, PF4708671, MK2206 and AZD6244 for another 24h. DMSO served as control. Apoptotic cells were identified by cleaved caspase 3 staining (green) in 2D and in spheroid sections. Apoptotic cells are indicated by white arrowheads. Nuclei are counterstained with DAPI (blue).

Supporting Figure SF4 (figshare) - Molecular evaluation of PI3K/AKT/mTOR- and RAS/RAF/MAPK-signaling in the presence or absence of inhibitory compounds. DLD-1 colon cancer cells, grown in 2D and 3D for 24h, were treated with DMSO, which served as control, Rapamycin, the pan mTOR inhibitor Torin1, the S6K1 inhibitor PF4708671, the AKT inhibitor MK2206 and the MEK1 inhibitor AZD4266 for another 24h. Afterwards, 2D and 3D cultures were harvested and whole protein extracts were subjected for Western blot analysis of different proteins of the PI3K/AKT/mTOR- and RAS/RAF/MAPK-pathway. **A** biological replicate 2, **B** biological replicate 3. Detection of phospho-proteins is indicated by p- prior to and the phosphorylated amino acid is indicated behind the protein name. α-tubulin and GAPDH served as loading control.

Supporting Figure SF5 (figshare) - Molecular evaluation of PI3K/AKT/mTOR- and RAS/RAF/MAPK-signaling in the presence or absence of inhibitory compounds.

Journal of Cell Science • Supplementary information

HCT116 colon cancer cells, grown in 2D and 3D for 24h, were treated with DMSO, which served as control, Rapamycin, the pan mTOR inhibitor Torin1, the S6K1 inhibitor PF4708671, the AKT inhibitor MK2206 and the MEK1 inhibitor AZD4266 for another 24h. Afterwards, 2D and 3D cultures were harvested and whole protein extracts were subjected for Western blot analysis of different proteins of the PI3K/AKT/mTOR- and RAS/RAF/MAPK-pathway. **A** biological replicate 1, **B** biological replicate 2. Detection of phospho-proteins is indicated by p- prior to and the phosphorylated amino acid is indicated behind the protein name. α-tubulin and GAPDH served as loading control.

Supporting Figure SF6 (figshare) - Molecular evaluation of PI3K/AKT/mTOR- and RAS/RAF/MAPK-signaling in the presence or absence of inhibitory compounds. Caco-2 colon cancer cells, grown in 2D and 3D for 24h, were treated with DMSO, which served as control, Rapamycin, the pan mTOR inhibitor Torin1, the S6K1 inhibitor PF4708671, the AKT inhibitor MK2206 and the MEK1 inhibitor AZD4266 for another 24h. Afterwards, 2D and 3D cultures were harvested and whole protein extracts were subjected for Western blot analysis of different proteins of the PI3K/AKT/mTOR- and RAS/RAF/MAPK-pathway. **A** biological replicate 1, **B** biological replicate 2. Detection of phospho-proteins is indicated by p- prior to and the phosphorylated amino acid is indicated behind the protein name. α-tubulin and GAPDH served as loading control.

Supporting Figure SF7 (figshare) - Gradual decrease of rpS6 phosphorylation from the outside to the inner core of DLD-1 spheroids. DLD-1 colon cancer cells were grown in 2D and 3D conditions for 24h and treated with DMSO, Rapamycin, Torin1, PF4708671, MK2206 and AZD6244 for another 24h. Representative images of p-rpS6 S240/244 immunohistochemistry staining (chromogen: diaminobenzidine, brown) of DLD-1 cells cultured on filter membranes and as spheroids (cross sections, 5 µm). Scale bars: 20 µm.

Supporting Figure SF8 (figshare) - Different spheroid formation time does not alter phenotypes in 3D. **A** DLD-1 colon cancer cells were seeded at different cell numbers for spheroid formation (1000, 1500, 2000, 3000) and these spheroids were for different time periods in order to reach the same spheroid size prior to experimentation (e.g. 3000 cells were incubated for 24 hrs, whereas 1000 cells were incubated for 96 hrs to reach the same sphere size). The initial differences of spheroid sizes are shown below in A after 24 hrs. After 24, 48 and 72 hrs of further incubation spheroids formed by 2000, 1500 and 1000 cells, respectively, reached the same size as 3000 cells after 24 hrs. **B** These spheroids of the same size but with different spheroid formation periods were then subjected to cell cycle analysis (EdU incorporation) and DNA staining (7-AAD) and displayed no apparent differences in cell cycle distribution. **C** To generalize these observations the same experimental approach was repeated with HCT116 cells and showed the same results.

Supporting Figure SF9 (figshare) - The presence of methylcellulose does not affect treatment response. DLD-1 colon cancer cells, grown in 2D and 3D for 24h, were treated with DMSO, which served as control, Rapamycin, the pan mTOR inhibitor Torin

and the AKT inhibitor MK2206 for further 24h in the presence or absence of 0.3% methylcellulose. Spheroid formation was carried out in ultra low attachment plates (96 well U-shaped, Thermo Scientific) to avoid cell attachment in the absence of methylcellulose. 2D and 3D cultures were harvested and whole protein extracts were subjected to Western blot analysis of different proteins of the PI3K/AKT/mTOR pathway. No difference in Akt and S6 phosphorylation was detected in methylcellulose containing culture conditions versus methylcellulose free incubation in DMSO controls and in Torin1 or MK2206 treated cells.

Supplementary Table S1 - Mutational status

	CaCo-2	LS174T	DLD-1	HT29	HCT116	SW620	
MS status	MSS	**MSI**	**MSI**	MSS	**MSI**	MSS	27
CRC transcriptional subtype	Stem	Goblet	Stem	Goblet	Stem	Transit amplifying	27, 28
APC	**p.Q1367*** [1]	wt [2,3]	**p.I1417fs*2** [4]	**1)p.E853*** [1], **2)p.T1556fs*** [1,2], **3) p.E853*** [2]	wt [1,2]	**p.Q1338*** [4]	
CTNNB1	**1) -** [7], **2) p.G245A** [8]	**p.S45F** [2,3]	wt [8]	wt [2,8]	**p.S45del** [2]	wt [7]	
KRAS	wt [5,6]	**p.G12D** [2,3]	**p.G13D** [21]	wt [2,5]	**p.G12D** [2, 24]	**p.G12V** [25]	
HRAS	wt	wt	wt	wt	wt	wt	28
NRAS	wt	wt	wt	wt	wt	wt	28
BRAF	wt [5,6]	wt [2,3]	wt [17]	**p.V600E** [2,5,6]	wt [2]	wt [3]	
MAP2K4	-	-	-	wt [2]	wt	p.?	
EGFR	wt [9]	wt [2,3]	wt [18]	wt [2, 9,18]	wt	wt [9]	
EP300	wt [10]	-	**p.E1014*** [19]	**p.M1470fs*3** [10]	**1) p.M1470fs*3** [10], **2) p.N1700fs*9** [10]	wt [10]	
H3K27 demethylase	-	**p.E1316fs** [2,3]	-	-	wt [2]	-	
IDH1	-	-	**p.G97D** [20]	**wt** [2]	-	**wt** [20]	
PTEN	positive	positive	positive	positive	positive	positive	28
PIK3CA	wt [12]	**p.H1047R** [2,3]	**E545K** [22]	**p.P449T** [2]	**p.H1047R** [2]	wt [12]	
MLH1	-	wt [2,3]	-	wt [2]	**p.S252*** [2]	wt [2]	
MLL3	wt [11]	-	**p.G3438D** [11]	-	-	wt [11]	
CDKN2A(p16Ink4, p19 ARF)	-	wt [2,3]	-	-	**1) p.R24fs*20** [2], **2) p.G23fs/?** [24], **3) p.E74fs*15** [2]	wt	
SMAD4	**p.D351H** [13]	wt [2,3]	wt [13]	**p.Q311*** [2,13]	wt [2, 13]	**?**	
SMO	wt [14]	-	**p.T640A** [14]	wt [2, 14]	-	wt [14]	
TP53	**1) p.Glu204X** [15], **2) -** [16]	-	wt [23]	**p.R273H** [2]	wt [2]	**1) p.R273H, 2) p.P309S**	

References

1 Rowan AJ et al, Proc Natl Acad Sci U S A (2000) Mar 28;97(7):3352-7
2 van Haaften G et al, Nat Genet (2009) May;41(5):521-3
3 Papaemmanuil E et al, N Engl J Med (2011) Oct 13;365(15):1384-95
4 Homfray TF et al, Hum Mutat (1998) 11(2):114-20
5 Hinoue T et al, PLoS One (2009) Dec 21;4(12):e8357
6 Oliveira C et al, Oncogene (2003) Dec 11;22(57):9192-6
7 Ikenoue T et al, Jpn J Cancer Res (2002) Nov;93(11):1213-20
8 Ilyas M et al, Proc Natl Acad Sci U S A (1997) Sep 16;94(19):10330-4
9 Yuan Z et al, Cancer Res (2009) Oct 1;69(19):7811-8
10 Bryan EJ et al, Int J Cancer (2002) Nov 10;102(2):137-41
11 Watanabe Y et al, PLoS One (2011) 6(8):e23320
12 Arcaroli JJ et al, Clin Cancer Res (2012) May 1;18(9):2704-14
13 Fleming NI et al, Cancer Res (2013) Jan 15;73(2):725-35
14 Guleng B, J Gastroenterol (2006) Dec;41(12):1238-9
16 Djelloul S et al, FEBS Lett (1997) Apr 14;406(3):234-42
18 Kimura et al, Oncol Rep (2006) May;15(5):1205-10
19 Gayther SA et al, Nat Genet (2000) Mar;24(3):300-3
20 Bleeker FE et al, Hum Mutat (2009) Jan;30(1):7-11
21 Ikehara N et al, Int J Cancer (2005) Jul 20;115(6):943-50
23 Peinado M et al, Int J Oncol (1993) Feb;2(2):123-34
24 Gayet J et al, Oncogene (2001) Aug 16;20(36):5025-32
25 Janakiraman M et al, Cancer Res (2010) Jul 15;70(14):5901-11
26 Sadanandam, A. et al. Nat. Med. (2013), 19 619–625
27 Medico, E et al, Nat. Comm. 2015, DOI: 10.1038/ncomms8002

Supplementary Table S2 - Primary and secondary antibodies

Name	Company	Cat#	Clone#	Dilution	
Primary antibody				*Immunoblot*	*IF, IHC*
p-Akt T308-XP®	Cell Signaling Technology	13038	D25E6	1:1000	-
p-Akt S473-XP®	Cell Signaling Technology	4060	D9E	1:1000	1:100
Akt pan	Cell Signaling Technology	2920	40D4	1:2000	-
p-PRAS40 T246	Cell Signaling Technology	2640	-	1:1000	-
4E-BP1	Cell Signaling Technology	9452	-	1:1000	-
p-PKC (pan) β S660	Cell Signaling Technology	9371	-	1:1000	-
p-ERK1/2 T202/Y204-XP®	Cell Signaling Technology	4370	D13.14.4E	1:1000	1:300
ERK1/2	Cell Signaling Technology	4695	137F5	1:1000	-
p-p70 S6K T389	Cell Signaling Technology	9234	108D2	1:1000	-
p70 S6K c-term	Cell Signaling Technology	9202	-	1:1000	-
p-rpS6 S240/244	Cell Signaling Technology	2215	-	1:1000	-
p-rpS6 S240/244-XP®	Cell Signaling Technology	5364	D68F8	-	1:800
rpS6	Cell Signaling Technology	2317	54D2	1:1000	-
p-Rb S807/811	Cell Signaling Technology	9308	-	1:1000	-
KI67	Cell Signaling Technology	9449	8D5	-	1:400
IRS1	Cell Signaling Technology	2382	-	1:1000	-
Cytokeratin 18	Dako	M7010	DC10	-	1:50
CD31	Dako	M0823	JC70A	-	1:100
E-Cadherin	abcam	ab1416	HECD-1	1:1000	1:100
α Tubulin	Calbiochem	CP06	DM1A	1:5000	-
GAPDH	Trevigen	2275-PC-100	-	1:10,000	-
Secondary antibody					
anti-mouse IgG-heavy and light chain antibody, HRP conjugate	Bethyl Laboratories Inc.	A90-116P	-	1:10,000	-
anti-rabbit IgG-heavy and light chain antibody, HRP conjugate	Bethyl Laboratories Inc.	A120-101P		1:10,000	-
anti-rabbit IgG (H+L) antibody, AlexaFluor® 488 conjugate	Thermo Scientific Lab.	A-11034		-	1:500
anti-mouse IgG (H+L) antibody, AlexaFluor® 546 conjugate	Thermo Scientific Lab.	A-11030		-	1:500
anti-rabbit IgG antibody, biotinylated	Vector Laboratories	BA-1100		-	1:500

Supplementary Table S3

Click here to Download Table S3